

Photo-Chemical Evolution of Elliptical Galaxies

I. The high-redshift formation scenario

Antonio Pipino,¹ and Francesca Matteucci,¹

¹*Astronomy Department, University of Trieste, Via G.B. Tiepolo, 11, I-34127, Trieste, Italy*

Accepted, Received

ABSTRACT

In this paper we compute new multi-zone photo-chemical evolution models for elliptical galaxies, taking into account detailed nucleosynthetic yields, feedback from supernovae and an initial infall episode. By comparing model predictions with observations, we derive a picture of galaxy formation in which the higher is the mass of the galaxy, the shorter are the infall and the star formation timescales. Therefore, in this scenario, the most massive objects are older than the less massive ones, in the sense that larger galaxies stop forming stars at earlier times. Each galaxy is created outside-in, i.e. the outermost regions accrete gas, form stars and develop a galactic wind very quickly, compared to the central core in which the star formation can last up to ~ 1.3 Gyr. In particular, we suggest that both the duration of the star formation and the infall timescale decrease with galactic radius. In order to convert theoretical predictions into line-strength indices, different calibrations are adopted and discussed, focussing in particular on their dependence on the α -enhancement.

By means of our model, we are able to match the observed mass-metallicity and color-magnitude relations for the center of the galaxies as well as to reproduce the overabundance of Mg relative to Fe, observed in the nuclei of bright ellipticals, and its increase with galactic mass. Furthermore, we find that the observed Ca underabundance relative to Mg can be real, due to the non-negligible contribution of type Ia SN to the production of this element. We predict metallicity and color gradients inside the galaxies which are in good agreement with the mean value of the observed ones.

Finally, we conclude that models with Salpeter IMF are the best ones in reproducing the majority of the properties of ellipticals, although a slightly flatter IMF seems to be required in order to explain the colors of the most massive galaxies.

Key words: galaxies: ellipticals: chemical abundances, formation and evolution

1 INTRODUCTION

Any model of galaxy evolution presented so far had to overcome the strong challenge represented by the observational fact that elliptical galaxies show a remarkable uniformity in their photometric and chemical properties. The first proposed scenario of elliptical formation was the so-called monolithic collapse scenario (Larson 1974; Matteucci & Tornambe', 1987; Arimoto & Yoshii, 1987, AY; Chiosi & Carraro, 2002). In this framework, ellipticals are assumed to have formed at high redshift as a result of a rapid collapse of a gas cloud. This gas is then rapidly converted into stars by means of a very strong burst, followed by a galactic wind powered by the energy injected into the interstellar medium (ISM) by supernovae and stellar winds. The wind carries out the residual gas from the galaxies, thus inhibiting further star formation. Minor episodes of star formation, related to

gas accretion from the surrounding medium or interactions with neighbors, are not excluded although they do not influence the galactic evolution. On the other hand, thanks to the success of the cold dark matter theory in reproducing the anisotropy of the Cosmic Microwave Background, an alternative scenario of galaxy formation based on the Hierarchical Clustering scenario for the formation of dark matter halos was proposed. Hierarchical semi-analytic models predict that ellipticals are formed by several merging episodes which trigger star-bursts and regulate the chemical enrichment of the system (White & Rees, 1978). In this picture massive ellipticals form at relatively low redshifts through major mergers between spiral galaxies (e.g. Kauffmann & White, 1993; Kauffmann & Charlot, 1998).

In the following we will refer to the monolithic collapse as the model in which ellipticals formed relatively quickly and at high redshift as opposed to the hierarchical clustering

scenario where ellipticals are believed to form over a large redshift interval.

The high redshift formation of ellipticals is supported by observations showing an increase in the strength of the metal absorption lines (Mass-Metallicity relation, e.g. Carollo et al., 1993; Gonzalez, 1993; Davies et al., 1993; Trager et al. 1998, 2000) and a reddening of the stellar light (Color-Magnitude relation, hereafter CMR, Bower et al., 1992) with the velocity dispersion of the galaxies. If we interpret the measure of the spectral indices as a measure of the metallicity by means of a suitable calibration, we derive a picture in which these two relations can be explained primarily as a metallicity sequence (Kodama & Arimoto 1997). In other words, the most massive ellipticals are also the most metal rich. This fact was interpreted by Larson (1974) as due to the galactic winds which should occur later in the most massive objects, thus allowing the star formation process to continue for a longer period than in small galaxies. In particular, the higher is the mass of the galaxy, the larger is the chemical enrichment, the redder are the colors. However, this interpretation based on the galactic winds has been changed in the last years, owing to the observed $[\text{Mg}/\text{Fe}]$ ratio in the central parts of ellipticals and its trend with galactic mass. In the last decade there was an increasing evidence that $[\text{Mg}/\text{Fe}]$ ratio is larger than zero in the core of bright galaxies (e.g. Faber et al., 1992; Carollo et al., 1993; Davies et al., 1993; Worthey et al., 1992), suggesting that the star formation lasted for a period shorter than the time at which the pollution from type Ia SNe becomes important (see Weiss et al., 1995). In fact, an overabundance of Mg relative to Fe is the clear sign that a short process of galaxy formation occurred before than a substantial number of type Ia SNe could explode and contribute to lower the $[\text{Mg}/\text{Fe}]$ ratio (time-delay model, see Matteucci 2001). In addition, the $[\text{Mg}/\text{Fe}]$ ratio in the cores of ellipticals increases with galactic mass (Worthey et al. 1992; Weiss et al. 1995; Kuntschner 2000, 2001) indicating, among the possible solutions, that the star formation lasted for a shorter period in the more massive systems ('inverse wind', Matteucci 1994). This is clearly at variance with the 'classical wind scenario' of Larson. Other possible solutions to the increase on $[\text{Mg}/\text{Fe}]$ as a function of galactic mass are a variable IMF and/or a decrease of the dark matter content as a function of galactic mass (see Matteucci et al., 1998).

On the other hand, recent models with selective merging (i.e. large galaxies merge only with large galaxies) were able to reproduce the $\text{Mg}-\sigma$ relation (e.g. Worthey & Collobert, 2003) and the CMR (e.g. Kauffmann & Charlot, 1998), but they still cannot explain the $[\text{Mg}/\text{Fe}]$ -mass relation (Thomas et al. 1999, Thomas & Kauffmann 1999, Kuntschner 2000).

Moreover, line-indices and color gradients are observed in ellipticals (e.g. Carollo et al., 1993; Peletier et al., 1990). Also in this case, they can be reproduced by means of a variation in the mean metallicity of the stellar population as a function of the radius (Tantalo et al., 1998b; Martinelli et al., 1998; Tamura et al., 2000) in the context of monolithic models, whereas hierarchical assembly of galaxies seems to produce milder slopes than the observed ones (e.g. Bekki & Shioya, 1999).

One of the main characteristics which makes ellipticals a very appealing test bench for any scenario of galaxy formation, is that they exhibit tight relations not only in the

chemical properties, but also in the dynamical ones. It is well known that elliptical galaxies populate a plane (Fundamental Plane, FP) in the space defined by the effective radius (R_{eff}), the mean surface brightness within R_{eff} and the central velocity dispersion σ (Dressler et al., 1987; Djorgovski & Davies, 1987; Bender et al., 1992; Burstein et al. 1997). In particular, cluster ellipticals show a very small scatter around the FP and such a tight scaling relation is interpreted as an evidence of a highly standardized and synchronized formation of these galaxies. Formation of ellipticals at high redshift can reasonably explain the tightness of this plane, whereas predictions based on hierarchical models seem to be at odds with dynamical evidences deriving from the study of the FP, at least in the case of non-dissipative merging (e.g. Nipoti et al., 2002, 2003). From a dynamical perspective, evidences favouring the hierarchical scenario are represented by the observed interacting galaxies (ongoing mergers), ellipticals with disturbed morphologies (i.e. counter-rotating cores, dust lanes, ripples, e.g. Kormendy & Djorgovski, 1989), the morphology-density relation in clusters (Dressler et al., 1997) and the Butcher-Oemler effect (Butcher & Oemler, 1978, although it could be related only to lenticular galaxies).

Thanks to the new generation telescopes, the above-mentioned relations for the local universe are found to hold also at high redshift. In particular, recent observations of the lack of significant change in the slope and in the scatter of the CMR (Stanford et al., 1998), the slow evolution of colors (e.g. Saglia et al. 2000; Ellis et al., 1997), mass to light ratios (e.g. van Dokkum & Franx, 1996; Rusin et al., 2003; van de Ven et al., 2003) and line strength indices of cluster early-type galaxies out to $z \sim 1$ (e.g. Bernardi et al., 2003; van Dokkum et al. 1998) suggest that their stars were formed at high redshift ($z > 3$) in a well synchronized epoch, and then evolved quiescently. In summary, many observations (see Peebles 2002 for a review) suggest that ellipticals could already be in place at $z \sim 2 - 3$, and their high-redshift counterpart could be represented by Lyman Break Galaxies (Steidel et al., 1996a,b) which show chemical abundances and star formation rates consistent with those of a rapidly evolving elliptical in their early evolutionary phases (e.g. Matteucci & Pipino, 2002), or by Extremely Red Objects (EROs, e.g. Daddi et al., 2000; Miyazaki et al., 2003).

Peebles (2002) critically reviewed the still standing problems and the differences between these two competing scenarios for galaxy formation, pointing out that this classification is now becoming meaningless, surviving only in historical sense (for another very recent review see de Freitas Pacheco et al., 2003), since probably the best way to explain the whole set of observables within a cosmological framework would request both scenarios to converge. Therefore, in order to shed light on this issue, this paper represents the first in a series in which we intend to investigate the formation and the evolution of elliptical galaxies and the role played by the SN feedback, infall timescale, star formation efficiency and stellar nucleosynthesis in driving the mass-metallicity and the color-magnitude relations, as well as the Mg overabundance and the radial gradients in metallicity and colors.

In particular, in this article we present a new photochemical evolution model for ellipticals, in which, for the first time, the inverse wind scenario plus an initial infall

episode are adopted within a multi-zone formulation. The model results are then compared with the observations, in order to fix the best set for our input parameters and to define the best model. Under reasonable assumptions on the behaviour of the infall timescale and the star formation efficiency with galactic mass, we show how this kind of model can reproduce the whole set of chemical and photometric observables simultaneously.

In the forthcoming papers we shall compare our best-model results with those from a hierarchical formation scenario, merger-induced starburst, prolonged star formation, and we shall make predictions for X-ray halos of ellipticals and the chemical enrichment of the intra-cluster medium. This paper is organized as follows: in section 2 we present the model. Section 3 is dedicated to the photo-chemical properties. In section 4 we discuss the results and draw the conclusions for our best model. In the following, conversion from cosmic time to redshift is done for a cosmological model with $\Omega_m = 0.3$, $\Omega_\Lambda = 0.7$ and $H_o = 70 \text{ km s}^{-1} \text{ Mpc}^{-1}$. For all models we assume a redshift of formation of 5. Under this assumption we have an age of $\sim 12.3 \text{ Gyr}$ for our model galaxies. This age has been chosen in order to reproduce the observed CMR.

2 THE MODEL

The adopted chemical evolution model is an up-dated version of the multi-zone model of Martinelli et al. (1998) and Pipino et al. (2002), in which we divide an elliptical galaxy into several non-interacting shells. In particular, we use spherical shells with a fixed thickness of $0.1 R_{eff}$, where R_{eff} is the galactic effective radius, and limit our analysis to $10 R_{eff}$, unless otherwise stated. In the following we refer to the $0 - 0.1 R_{eff}$ as the central zone, or the galactic core. For each shell we calculate the evolution of the elemental abundances by means of the equation of chemical evolution:

$$\begin{aligned} \frac{dG_i(t)}{dt} = & -\psi(t)X_i(t) + \\ & + \int_{M_L}^{M_{Bm}} \psi(t - \tau_m) Q_{mi}(t - \tau_m) \phi(m) dm + \\ & + A \int_{M_{Bm}}^{M_{BM}} \phi(m) \left[\int_{\mu_{min}}^{0.5} f(\mu) \psi(t - \tau_{m_2}) d\mu \right] dm + \\ & + (1 - A) \int_{M_{Bm}}^{M_{BM}} \psi(t - \tau_m) Q_{mi}(t - \tau_m) \phi(m) dm + \\ & + \int_{M_{BM}}^{M_U} \psi(t - \tau_m) Q_{mi}(t - \tau_m) \phi(m) dm + \\ & + \left(\frac{dG_i(t)}{dt} \right)_{infall}, \end{aligned}$$

where $G_i(t) = \rho_{gas}(t) X_i(t) / \rho_{gas}(0)$ is the mass density of the element i at the time t normalized to the initial value of the gas density. $X_i(t)$ is defined as the abundance by mass of the element i . By definition $\sum_i X_i = 1$. We refer the reader to Matteucci & Gibson (1995) and Matteucci & Greggio (1986) for a comprehensive discussion of this equation. Here we recall that the integrals in the right-hand side of the equation give the rate at which the element i is restored into the interstellar medium (ISM) as unprocessed or newly-

synthesized element by low- and intermediate-mass stars, SNIa and SNII, respectively. The last term represents the infall rate, namely the rate at which the gas is assembling to form the galaxy.

The variable ψ is the star formation rate, for which we adopted the following law:

$$\psi(t) = \nu \cdot \rho_{gas}(t), \quad (1)$$

namely it is assumed to be proportional to the gas density via a constant ν which represents the star formation efficiency. We assume ν as an increasing function of the galactic mass (see Tables 1, 2 and 3) in order to reproduce the 'inverse wind model' (Matteucci, 1994, Matteucci et al., 1998). The star formation history of a particular shell is thus determined by the interplay between the infall timescale at that radius, the star formation efficiency and the occurrence of the galactic wind (i.e. the energetic feedback from SNe and stellar winds). In each zone we assume that $\psi = 0$ after the development of the wind.

$\phi(m) \propto m^{-(1+x)}$ is the initial mass function (IMF), normalized to unity in the mass interval $0.1 - 100 M_\odot$. In the following we shall use only the exponents $x=1.35$ (Salpeter, 1955) and $x=0.95$ (AY).

One of the fundamental points upon which our model is based, is the detailed calculation of the SN explosion rates. For type Ia SNe we assume a progenitor model made of a C-O white dwarf plus a red giant (Whelan & Iben, 1973), then we have:

$$R_{SNIa} = A \int_{M_{Bm}}^{M_{BM}} \varphi(M_B) \int_{\mu_m}^{0.5} f(\mu) \psi(t - \tau_{M_2}) d\mu dM_B, \quad (2)$$

(Greggio & Renzini, 1983; Matteucci & Greggio, 1986), where M_B is the total mass of the binary system, $M_{Bm} = 3M_\odot$ and $M_{BM} = 16M_\odot$ are the minimum and maximum masses allowed for the adopted progenitor systems, respectively. $\mu = M_2/M_B$ is the mass fraction of the secondary, which is assumed to follow the distribution law:

$$f(\mu) = 2^{1+\gamma} (1 + \gamma) \mu^\gamma. \quad (3)$$

Finally, μ_m is its minimum value and $\gamma = 2$. The predicted type Ia SN explosion rate is constrained to reproduce the present day observed value (Cappellaro et al., 1999), by fixing the parameter A in eq. (2). In particular, A represents the fraction of binary systems in the IMF which are able to give rise to SN Ia explosions. In the following we adopt $A = 0.18$ (0.05) for a Salpeter (AY) IMF.

On the other hand, the type II SN rate is:

$$\begin{aligned} R_{SNII} = & (1 - A) \int_8^{16} \psi(t - \tau_m) \varphi(m) dm \\ & + \int_{16}^{M_U} \psi(t - \tau_m) \varphi(m) dm, \end{aligned} \quad (4)$$

where the first integral accounts for the single stars in the range $8-16M_\odot$, and M_U is the upper mass limit in the IMF.

2.1 Energetics

2.1.1 Binding Energy

We evaluated the binding energy of the gas in the i -th zone as

$$E_{Bin}^i(t) = \int_{R_i}^{R_{i+1}} dL(R), \quad (5)$$

where $dL(R)$ is the work required to carry a quantity $dm = 4\pi R^2 \rho_{gas} dR$ of mass out to infinity and R_i is the radius of the i -th shell (Martinelli et al., 1998). The baryonic matter (i.e. star plus gas) is assumed to follow the distribution (Jaffe, 1983):

$$F_i(r) \propto \frac{r/r_o}{1 + r/r_o}, \quad (6)$$

where $r_o = R_{eff}/0.763$.

We assume that the dark matter (DM) is distributed in a diffuse halo ten times more massive than the baryonic component of the galaxy with a scale radius $R_{dark} = 10R_{eff}$ (Matteucci 1992), where R_{eff} is the effective radius. The DM profile is taken from Bertin et al. (1992). Other cases with a more concentrated DM lead to delayed winds and thus to prolonged star formation, at odds with observations (Martinelli et al. 1998).

2.1.2 Feedback from Supernovae

We adopt two different recipes for SNIa and SNII, respectively. For SNII we assume that the evolution of the energy in the 'snowplow' phase is regulated by Cioffi et al. (1988) cooling time. This timescale takes into account the effect of the metallicity of the gas, and therefore, one can model in a self-consistent way the evolution of a SNR in the ISM. Due to significant cooling by metal ions, only a few percent of the initial $\sim 10^{51}$ erg (blast wave energy) can be provided to the ISM. On the other hand, for type Ia SNe, we follow the suggestions put forward by Recchi et al. (2001) in the modelling of dwarf galaxies. Recchi et al. (2001) assume that, since SNIa explosions occur in a medium already heated by SNII, they contribute with the total amount of their energy budget (10^{51} erg), without radiative losses. This result has been already adopted by Pipino et al. (2002), who reproduced realistic models for ellipticals and the Fe abundance in the ICM. However, Pipino et al. (2002) stressed that, owing to the larger number of SNII relative to SNIa, the typical efficiency of energy release to the ISM averaged on both types of SN is $\sim 20\%$. Since we use a chemical evolution code which adopts the same formulation for the feedback as in Pipino et al. (2002), we consider a $\sim 20\%$ mean efficiency in energy transfer as a representative value also for the model galaxies presented in this paper.

We define the time when the galactic wind occurs (t_{gw}) as the solution of the following equation:

$$E_{th}^i(t_{gw}) = E_{Bin}^i(t_{gw}), \quad (7)$$

2.2 Infall

The main novelty of this paper relative to our previous ones (Matteucci et al., 1998; Martinelli et al., 1998; Pipino et al., 2002) is that we simulate the creation of the spheroid as due to the collapse of either a big gas cloud or several smaller gas lumps. The infall term in the chemical modelling of ellipticals was first introduced by Tantaló et al. (1996) and Kodama & Arimoto (1997) following a suggestion of Bressan et

al. (1994), in order to solve a problem similar to the 'Classical G-Dwarfs Problem' (e.g. Tinsley 1980) in the Milky Way. In particular, Bressan et al. (1994; see also Worthey et al., 1996) claimed that the UV-excess predicted by their theoretical spectral energy distribution (SED) could be reconciled with the observed one only by reducing the excess of low-metal stars. This can be done by relaxing the closed-box approximation and introducing an initial infall of gas which modulates the star formation, thus preventing the formation of too many low metallicity stars. The infall makes the star formation rate to start from a smaller value than in the closed box case, to reach a maximum and, then, to decrease when the star formation process becomes dominant. This treatment is certainly more realistic since it includes the simulation of a gas collapse.

The infall term is present in the right-hand side of the equation of the chemical evolution, and the adopted expression is:

$$\left(\frac{dG_i(t)}{dt}\right)_{infall} = X_{i,infall} C e^{-\frac{t}{\tau}}, \quad (8)$$

where $X_{i,infall}$ describes the chemical composition of the accreted gas, assumed to be primordial. C is a constant obtained by integrating the infall law over time and requiring that $\sim 90\%$ of the initial gas has been accreted at t_{gw} (in fact, we halt the infall of the gas at the occurrence of the galactic wind). Finally, τ is the infall timescale. We note that models in which $\tau \rightarrow 0$ are equivalent to the standard closed box model with all the gas already in place when the star formation starts.

A novelty in our formulation is that we adopted a new approach to the gas accretion history. In fact, at variance with previous works where τ was a-priori related to the free-fall timescale (Tantaló et al., 1996; Romano et al., 2002), we decided to consider the infall timescale as a free parameter. In particular, we decided to tune τ in each zone of the galaxy by requiring our models to fit the metallicity and color gradients (for a detailed discussion see section 3.2), as well as the mass metallicity and the color-magnitude relations. In the following we show results for models with infall timescales assumed to be either constant or a decreasing function of the mass. On the other hand, we adopted in each model a star formation efficiency increasing with mass, in order to predict a [Mg/Fe] ratio increasing with galactic mass, as suggested by Matteucci (1994).

2.3 Stellar Yields

We follow in detail the evolution of 21 chemical elements and to do that we need to adopt specific prescriptions for the stellar nucleosynthesis. In particular, our nucleosynthesis prescriptions are:

(i) For single low and intermediate mass stars ($0.8 \leq M/M_{\odot} \leq 8$) we make use of the yields of van den Hoek & Groenewegen (1997) as a function of metallicity.

(ii) We use the yields by Nomoto et al. (1997) for SNIa which are assumed to originate from C-O white dwarfs in binary systems which accrete material from a companion (the secondary) and reach the Chandrasekar mass and explode via C-deflagration.

(iii) Finally, for massive stars ($M > 8M_{\odot}$) we adopt the yields of Thielemann et al. (1996, TNH96) which refer to

the solar chemical composition, and the yields of Woosley & Weaver (1995, WW95 hereafter) corresponding to the solar chemical composition. In particular, we assumed WW95 case A for stars with masses $< 30M_{\odot}$, and case B for $\geq 30M_{\odot}$. We also computed one case where the yields of Mg of WW95 were corrected as recently suggested by François et al. (2003) (case WW95m) to best fit the solar neighbourhood stars. In particular, we increased the contribution to the Mg by a factor of ~ 10 in the mass range $11 - 22M_{\odot}$ and lowered it by the same factor in stars with mass $> 22M_{\odot}$, relative to the original WW95 results. In the following we always refer to the TNH96 yields, unless otherwise stated.

2.4 Photometry

We calculate the detailed photometric evolution for elliptical galaxies of different baryonic mass (10^{10} , 10^{11} , $10^{12}M_{\odot}$) by applying the spectro-photometric code by Jimenez et al. (1998), where all the details can be found. In particular, we reconstruct the composite stellar population (CSP) inhabiting each zone of the galaxies, for which we know the star formation and chemical evolution history. In tables 1, 2 and 3 we show the predicted K- and B-band luminosities of the galaxy models, obtained by integrating the contributions of each zone out to $10 R_{eff}$ whereas the colors for the inner zone are plotted in Fig. 10.

2.5 Galactic models

We run models for elliptical galaxies in the baryonic mass range $10^{10} - 10^{12}M_{\odot}$. M_{lum} is the 'nominal' mass of the object, i.e. the mass of the initial gas budget (we recall that we normalize the infall law between $t = 0$ and $t \sim t_{gw}$). The mass in stars at the present time is $\sim 0.2 - 0.4 M_{lum}$ for all the models and the velocity dispersion σ is evaluated from the relation $M = 4.65 \cdot 10^5 \sigma^2 R_{eff} M_{\odot}$ (Burstein et al., 1997). The effective radius R_{eff} is the final one, achieved when the collapse is over and this occurs roughly at the time τ .

The models are:

- (i) Model I: Salpeter IMF, τ constant with galactic mass (see Table 1).
- (ii) Model II: Salpeter IMF, τ decreasing with galactic mass (see Table 2).
- (iii) Model III: as Model II, but with Arimoto & Yoshii IMF (see Table 3).

Moreover, for each model we considered the following cases:

- a: τ constant with radius.
- b: τ decreasing with radius.
- c: τ increasing with radius.

3 RESULTS

3.1 The $[\alpha/Fe]$ vs. $[Fe/H]$ relations

First of all we present the chemical properties predicted in the core of ellipticals. In particular, we show the behaviours of the main chemical species in the ISM of these galaxies.

Unfortunately, the only way to derive abundances in ellipticals is through metallicity indices measured in integrated stellar spectra. Therefore, in order to compare our results with observations, we need to transform our model predictions into line-strength indices (see section 3.1.1), thus adding possible sources of systematic errors. In the following we present our results concerning the real abundances expressed in the usual *bracket* notation, where solar abundances are taken from Anders & Grevesse (1989), unless otherwise stated.

The main parameters of Models I, II and III, as well as their predicted photo-chemical properties are shown in Tables 1, 2 and 3, respectively. In particular, in column 1 we present the luminous mass of the model. The assumed effective radius, star formation efficiency, infall timescale and galactic wind occurrence for the central (i.e. $0 - 0.1R_{eff}$) zone are shown in columns 2, 3, 4 and 5 respectively. In column 6 we show the Mg_2 index predicted by means of Tantalo et al.'s SSP (see next section), whereas in column 7 we present the predicted mean stellar $[< Mg/Fe >]_{*}$. The last two columns contain the predicted B- and K-band galactic luminosities. We stress that the values in the galactic core are constrained by the observed relations, so are the same in all the different cases (a, b and c). In other words, the results presented in these Tables are independent of the assumed relation between τ and the galactic radius. As expected from the assumed increase of ν with the galactic mass, in each model the galactic wind occurs earlier in the more massive galaxies. It is worth noting that in Larson's model (1974), as well as in Arimoto & Yoshii's (1987) and Matteucci & Tornambe's (1987) models, the efficiency of star formation was assumed to be constant or to decrease with galactic mass, thus leading to the situation of the classical wind scenario. In the core of the largest objects the active evolution stops at ~ 0.5 Gyr, whereas it can last more than 1 Gyr in the central regions of a $10^{10}M_{\odot}$ galaxy. As we shall see in section 3.1.2, this sequence in the development of the galactic winds is needed to reproduce the observed Mg enhancement relative to Fe in bright ellipticals. In our models τ and ν work together in the same direction, producing, in the more massive systems, a star formation rate peaked at earlier times and with higher peak values than in the smaller ones. The increase of the star formation efficiency, in spite of the shorter duration of the star formation process, leads to a higher metal enrichment in the most massive galaxies. Therefore, this mechanism preserves the mass-metallicity relation which was the main achievement of the classic wind models.

In Fig. 1 we plot the predicted curves for the $[\alpha/Fe]$ abundance ratios versus $[Fe/H]$ in the ISM of the central zone ($0 - 0.1R_{eff}$) for a $10^{11}M_{\odot}$ Model II galaxy. Similar trends are predicted by Model I, whereas we obtain systematically higher $[\alpha/Fe]$ ratios in the curves predicted by Model III, due to its flatter IMF. The high values ($[\alpha/Fe] > 1$) at very low metallicity are due to the adopted yields, as it can be clearly seen from Fig. 2 comparing Model II predictions (dotted curve) with those from Pipino et al. (2002) best model, adopting the yields of Woosley & Weaver (1995), which are systematically lower by $\sim 0.2 - 0.4$ dex. On the other hand, the α -element overabundance relative to Fe, and its decrease with increasing metallicity is due to the differ-

Table 1. Model I

M_{lum} (M_{\odot})	R_{eff} (kpc)	ν (Gyr^{-1})	τ (Gyr)	t_{gw} (Gyr)	Mg_2	$\langle [Mg/Fe] \rangle$	L_B ($10^{10} L_{\odot}$)	L_K ($10^{10} L_{\odot}$)
10^{10}	1	3	0.2	1.114	0.276	0.259	0.08	0.35
10^{11}	3	10	0.2	0.570	0.283	0.305	0.79	3.95
10^{12}	10	27	0.2	0.499	0.327	0.316	7.25	40.6

The values presented in this table are referred to the central ($0 \rightarrow 0.1R_{eff}$) zone of the models. The calibration used for Mg_2 is from Matteucci et al. (1998), see section 3. The luminosities are referred to the whole galaxy.

Table 2. Model II

M_{lum} (M_{\odot})	R_{eff} (kpc)	ν (Gyr^{-1})	τ (Gyr)	t_{gw} (Gyr)	Mg_2	$\langle [Mg/Fe] \rangle$	L_B ($10^{10} L_{\odot}$)	L_K ($10^{10} L_{\odot}$)
10^{10}	1	3	0.5	1.299	0.267	0.150	0.07	0.33
10^{11}	3	10	0.4	0.709	0.298	0.206	0.78	3.92
10^{12}	10	22	0.2	0.544	0.328	0.303	7.42	41.3

The values presented in this table are referred to the central ($0 \rightarrow 0.1R_{eff}$) zone of the models. The calibration used for Mg_2 is from Matteucci et al. (1998), see section 3. The luminosities are referred to the whole galaxy.

ent origin of these elements (time-delay model, Matteucci & Greggio, 1986, see section 2.3).

The α -elements exhibit different degrees of enhancement with respect to Fe. This is due, from a theoretical point of view, to the different degree of production of each element in type II and Ia SNe. In particular, Si and Ca show a lower overabundance relative to Fe than O and Mg. From an observational point of view, the measure of the CaII triplet in the near infrared is considered as a good tracer for the global metallicity, since it is independent from the age (e.g. Idiart et al. 1997). The observations show that, although Ca belongs to the α elements, the strength of the observed lines follows very closely $[Fe/H]$ instead of $[Mg/H]$ (Worthey, 1998; Trager et al., 1998; Saglia et al. 2003). In particular Thomas et al. (2003) suggested $[Ca/Mg] = -0.3$, and Saglia et al. (2003), after a detailed analysis of several possible sources of error, claimed that the Ca depletion in ellipticals might be real. Our calculations suggest $\langle [Ca/Mg] \rangle = -0.152$ and $\langle [Ca/Fe] \rangle = -0.03$ (these values are referred to the core of a $10^{11} M_{\odot}$ Model II galaxy). These results can be explained simply in terms of yields, since Ca is produced in a non-negligible amount by type Ia SNe. In fact, the mass of Ca ejected during a SNIa explosion in the model W7 (Nomoto et al., 1997) is $\sim 0.012 M_{\odot}$, whereas the contribution of type II SNe averaged on a Salpeter IMF in the mass range $10 - 50 M_{\odot}$ is $\sim 0.0058 M_{\odot}$ (see Table 3 of Iwamoto et al., 1999). Silicon, for the same reason of Ca, presents a very similar behaviour and a clear evidence of these departures from the α element abundance pattern (represented by O and Mg) at high $[Fe/H]$, as it can be seen in Fig. 1.

The behaviour of the $[O/Fe]$ abundance ratio in the ISM of several galactic models is analysed in Fig. 2, where we plot the new model results for different galactic masses compared to predictions from Pipino et al. (2002) best model. From Fig. 2 we infer a higher $[O/Fe]$ in the ISM of the larger galaxies at a fixed $[Fe/H]$, as a consequence of the effect of the more efficient star formation rate in the brightest galaxies relative to the smaller ones.

Finally, in Fig. 3, theoretical $[C/Fe]$ and $[N/Fe]$ abundance ratios in the ISM as functions of $[Fe/H]$ are shown

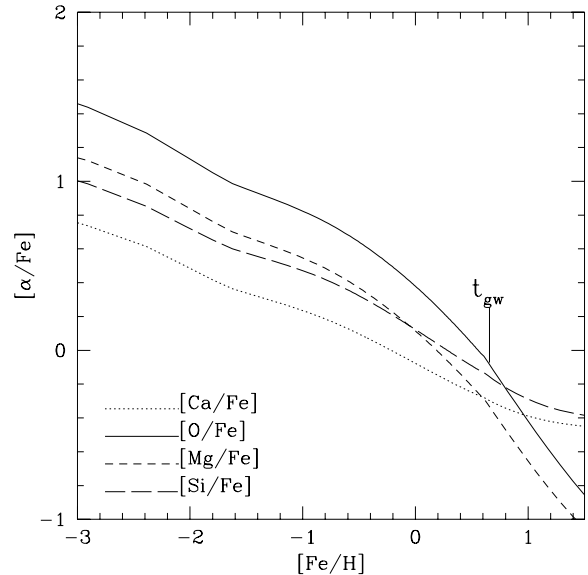


Figure 1. Theoretical $[O, Mg, Si, Ca/Fe]$ abundance ratios in the ISM as functions of $[Fe/H]$ predicted by Model II, for the core of a $10^{11} M_{\odot}$ galaxy. Solar value for O by Holweber (2001). The time for the occurrence of the galactic wind, t_{gw} , is indicated.

for the core of a $10^{11} M_{\odot}$ Model II galaxy. The fast increase of N abundance with metallicity is expected, since N produced in massive stars is assumed to be only secondary (but see recent calculations of Meynet & Maeder 2002, where a small fraction of primary N from massive stars is predicted). On the other hand, some primary N is produced in intermediate mass stars in the yields adopted here. C exhibits a monothonic decrease that parallels the $[O/Fe]$ behaviour although the predicted overabundance of C relative to Fe is much lower than for the α -elements and this is due to the fact that C is largely produced in low and intermediate mass stars.

Table 3. Model III

M_{lum} (M_{\odot})	R_{eff} (kpc)	ν (Gyr^{-1})	τ (Gyr)	t_{gw} (Gyr)	Mg_2	$\langle Mg/Fe \rangle$	L_B ($10^{10} L_{\odot}$)	L_K ($10^{10} L_{\odot}$)
10^{10}	1	5	0.3	1.234	0.421	0.534	0.03	0.39
10^{11}	3	14	0.2	0.650	0.429	0.535	0.38	4.66
10^{12}	10	27	0.1	0.504	0.453	0.581	4.00	50.0

The values presented in this table refer to the central ($0 \rightarrow 0.1R_{eff}$) zone of the models. The calibration used for Mg_2 is from Matteucci et al. (1998), see section 3. The luminosities refer to the whole galaxy.

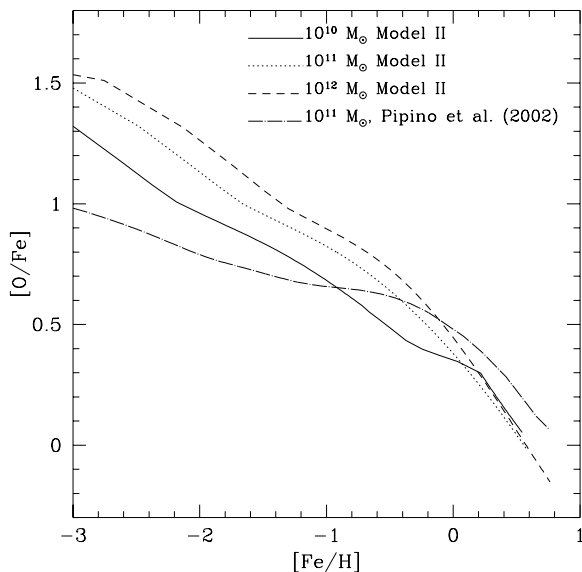


Figure 2. Theoretical $[O/Fe]$ abundance ratios in the ISM as functions of $[Fe/H]$ predicted by Model II for the core of $10^{10} - 10^{12} M_{\odot}$ galaxies. Solar value for O by Holweger (2001). Results for Pipino et al. (2002) best model galaxy of $10^{11} M_{\odot}$ are shown by a long-dashed-dotted line.

3.1.1 Mass-Metallicity relations for ellipticals

From the observational point of view, we infer the presence of the so-called mass-metallicity relation from the increasing strength of the metallic absorption lines with increasing velocity dispersion of the galaxy (e.g. Faber et al., 1977; Carollo et al., 1993; Gonzalez, 1993; Davies et al., 1993; Trager et al. 1998, 2000). At the present time, these relations are well established thanks to the increasing number of observed galaxies (e.g. Colless et al., 1999, give $Mg_2 = 0.257 \log \sigma - 0.305$, with an intrinsic scatter of 0.016 mag. On the other hand, Bernardi et al., 2003, with their huge sample of early type galaxies at $z < 0.3$, found $\log Mg_2 \simeq (0.20 \pm 0.02) \log \sigma$, with an intrinsic scatter of 0.011 mag, and $\log \langle Fe \rangle \simeq (0.11 \pm 0.03) \log \sigma$, with a scatter of 0.011).

In the following we focus on the two indices Mg_2 and $\langle Fe \rangle$, which are related to the metallicity of the observed object, but carry also information on its age (because of the well-known age-metallicity degeneracy, e.g. O’Connell, 1976).

The first step in order to compare our predicted abundances with the observed indices, is to compute the mean stellar abundance of the element X ($\langle X/H \rangle \simeq \langle Z_X \rangle$), defined as (Pagel & Patchett 1975):

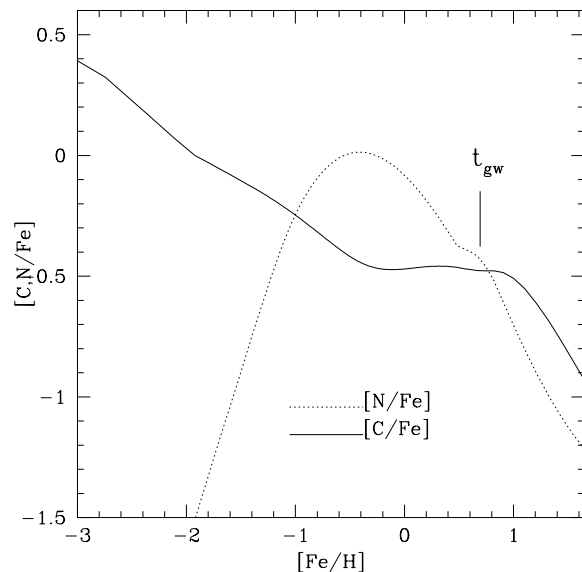


Figure 3. Theoretical $[C,N/Fe]$ abundance ratios in the ISM as functions of $[Fe/H]$ predicted by Model II for the core of a $10^{11} M_{\odot}$ galaxy.

$$\langle Z_X \rangle = \frac{1}{S_0} \int_0^{S_0} Z_X(S) dS, \quad (9)$$

where S_0 is the total mass of stars ever born contributing to the light at the present time. We recall that, for massive ellipticals, results obtained by averaging on the stellar mass are very similar to those obtained by averaging on the stellar luminosity at the present time (which is the right procedure, since the observed indices are weighted on V-band luminosity, see e.g. Arimoto & Yoshii, 1987; Matteucci et al., 1998). Tests on the $10^{11} M_{\odot}$ Model II galaxy confirm these findings. In particular, the differences between these two alternatives result into an offset of only a few percents in the predicted indices. Then, we transform our chemical information into indices by means of a *calibration* relation. We adopt the calibrations derived by Matteucci et al. (1998) from the synthetic indices of Tantalo et al. (1998a), which takes into account the Mg enhancement relative to Fe:

$$\begin{aligned} Mg_2 &= 0.233 + 0.217[Mg/Fe] \\ &+ (0.153 + 0.120[Mg/Fe]) \cdot [Fe/H], \\ \langle Fe \rangle &= 3.078 + 0.341[Mg/Fe] \\ &+ (1.654 - 0.307[Mg/Fe]) \cdot [Fe/H], \end{aligned}$$

for a stellar population 15 Gyr old. For comparative pur-

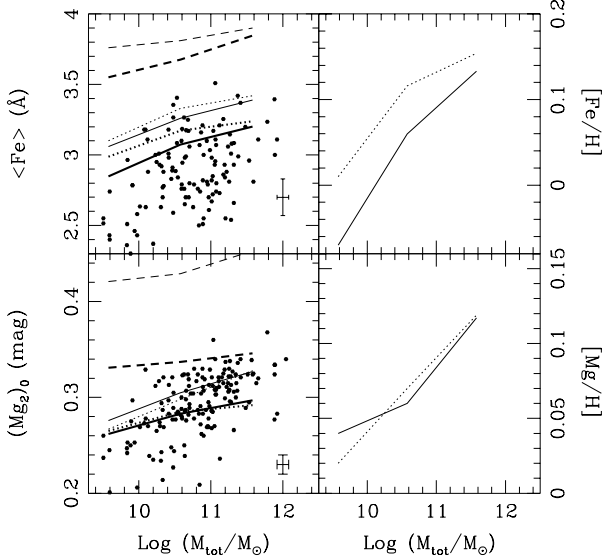


Figure 4. *Right:* Mg and Fe abundances in the stellar component predicted by Model I (solid) and Model II (dotted) as functions of galactic mass. *Left:* Line-strength indices predicted by Model I (solid), Model II (dotted) and Model III (dashed), using Tantalo et al. (1998a) and Worthey (1994) calibrations (thick and thin lines, respectively), plotted versus a collection of data from Carollo et al. (1993), Trager et al. (1998), Gonzalez (1993), Kuntschner (2000), Kuntschner et al. (2001). The typical errors are shown in the panels.

poses we use also the calibration relations of Worthey (1994) for a 12 Gyr old SSP with solar abundance ratios and $[Fe/H] > -0.5$.

These relations are:

$$Mg_2 = 0.187 \cdot [Fe/H] + 0.263,$$

$$\langle Fe \rangle = 1.74 \cdot [Fe/H] + 2.97,$$

In this way we can have a good estimate of the impact of α -enhancement in the predicted metallicity indices, and we are able to draw conclusions which are independent from the assumed calibration.

Our models with Salpeter IMF (solid and dotted curves in Fig. 4, representing Model I and II, respectively) fit reasonably well the observed mass-metallicity relations, although they predict a slightly flatter slope with respect to the observations. On the contrary, the model with AY IMF (dashed line) predicts too high values for the line-strength indices. The difference between the predicted slopes and the observed ones could be due to a too low predicted metallicity in our high mass models, which reflects in a lower Mg_2 than the observed one, but it could also depend on other factors including the difference between the *assumed* mass of the objects and that derived from the *observed* σ . Finally, it could be due to the adopted calibrations. In particular, from the bottom-left panel of Fig. 4, we note that the difference between Model I and II predictions for Mg_2 , for a fixed calibration relation, reflects in an offset of < 0.02 mag, being the slope of the mass-metallicity relations nearly the same.

On the other hand, the slopes are different when considering the two calibrations, and the predictions based on

α -enhanced tracks are systematically higher by $\sim 0.02 - 0.06$ mag. Going to numerical details, Model I predicts that Mg and Fe abundances variation (between the highest and the lowest mass model) are $\Delta[Mg/H] = 0.097$ dex (being oversolar in both cases) and $\Delta[Fe/H] = 0.203$ dex (see right-hand panels of Fig. 4). These results translate into a $\Delta Mg_2 = 0.046$ (Tantalo et al. calibration), $\Delta Mg_2 = 0.035$ (Worthey calibration) and $\Delta \log \langle Fe \rangle \simeq 0.05$ (for both calibrations). For Model II we obtain very similar results, the only differences being a somewhat flatter behaviour of $[Fe/H]$ ($\Delta[Fe/H] = 0.153$ dex) and a larger ΔMg_2 ($= 0.061$, Tantalo et al. calibration), whereas $\Delta Mg_2 = 0.027$ for the Worthey calibration. The main driver of this difference arises from the variation of the $[Mg/Fe]$ ratio, which increases faster in Model II than in Model I. This implies that our model predictions are not independent from the assumed calibration, but this fact is in general less important than a change in the IMF, as we can deduce by comparing the curves in Fig. 4 for Model III with the observed points. In fact, we rule out model III (AY IMF), whose predictions do not match the observed indices (Fig. 4) and since the entries in column 7 of Table 3 (to be compared with the expected $[Mg/Fe] \sim 0.2 - 0.4$ of Fig. 6) show a too high Mg overabundance. Model III fails in reproducing these quantities even if we assume an extremely short infall timescale and WW95 yields for massive stars, which give lower $[Mg/Fe]$. These results reinforce the need of a Salpeter IMF in order to reproduce the whole set of observables.

For what concerns the mass- $\langle Fe \rangle$ relation (always in Fig. 4), the lowest mass models predict in general a $\sim 0.2 - 0.3\text{\AA}$ higher $\langle Fe \rangle$ index than the average observed value, also when the Worthey calibration is considered. This disagreement could be either due to the adopted stellar yields, or to uncertainties in the data (see the large spread in the observations in Fig. 4, and in particular in the $\langle Fe \rangle$ index measurements which suffer larger uncertainties than those of Mg_2 . Typical values are $> 0.2\text{\AA}$).

Finally, in the right panels of Fig. 4 we show our predicted Fe-mass and Mg-mass relations, when real abundances and not indices are considered. The Figure indicates a slight flattening of the $[Fe/H]$ for the most massive ellipticals, which is not present in the predicted $[Mg/H]$. This can be due to the fact that in the inverse wind model picture larger galaxies develop galactic winds before the less massive ones and therefore the type Ia SNe have less time to restore Fe into the ISM.

3.1.2 $[Mg/Fe]$

A particular emphasis should be given to the observed increase in the enhancement of Mg with respect to Fe going to massive ellipticals (e.g. Worthey et al., 1992; Matteucci, 1994; Thomas, et al. 2002), since it represents a very strong constraint on their star formation history. One can envisage several possibilities to account for this trend: a shorter timescale of star formation which can be obtained by increasing the star formation efficiency with galactic mass which, in turn, induces the occurrence of galactic winds, with consequent loss of the residual gas, earlier in the most massive objects (inverse wind picture, see Matteucci 1994). Another possibility is to assume that the IMF varies from galaxy to galaxy becoming flatter with increasing galactic

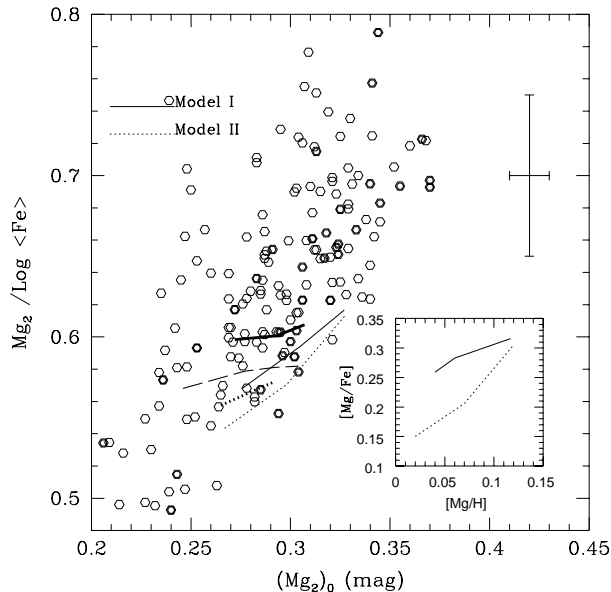


Figure 5. Predicted relations for Model I (solid), Model II (dotted) and a model with *classic* wind (Pipino et al., 2002, dashed) are shown. Indices obtained with the Tantaló et al. calibration are displayed with thick lines, whereas results obtained by means of the Worthey calibration are shown with thin curves. Data from Gonzalez (1993), Carollo et al. (1993), Kuntschner (2000), Kuntschner et al. (2001). The typical error is shown in the top-right corner. Mean stellar $[Mg/Fe]$ versus $[Mg/H]$ from the inner zones of Model I and II are shown in the small figure.

mass. Finally, a decreasing amount of dark matter with increasing luminous mass or a selective loss of metals could be the cause for the increase of $[Mg/Fe]$ (see Matteucci et al. 1998 for an extensive discussion). In this paper we consider only the first possibility, as already discussed in the previous sections.

In Fig. 5 we show the observed trend of Mg/Fe in elliptical galaxies by means of the quantity $Mg_2/\log < Fe >$ plotted versus $(Mg_2)_0$ (as a mass tracer) and our model curves. We recall here that Mg_2 is defined in magnitudes, whereas $< Fe >$ is in \AA , so in order to have consistent variations (i.e. on the same scale) of the two indices, we decided to use $\log < Fe >$ as a tracer for $[Fe/H]$. Although there is a good agreement between the predicted and the observed slopes, our curves lie under the mean relation expected from the fit to the observed values. This is a consequence of the slightly higher $< Fe >$ predicted by our models (see top-left panel of Fig. 4 and related discussion). We emphasize that the inverse wind model is necessary to reproduce the observed slope in the relations involving α -elements and Fe. In fact, we see that the trend for $Mg_2/\log < Fe >$ vs. $(Mg_2)_0$ relation predicted by a *classic* wind model (dashed line in Fig. 5), with similar input parameters (see also Pipino et al. 2002 for the details of this model), is at variance with the observed behaviour. Note, however, the large uncertainty affecting this kind of diagnostic. In the small panel we show for comparison the predicted trends for the *real* abundances in the stellar populations of our galactic models.

In Fig. 6 we present our predictions for the mean stellar $[Mg/Fe]$ plotted against a set of data analysed and trans-

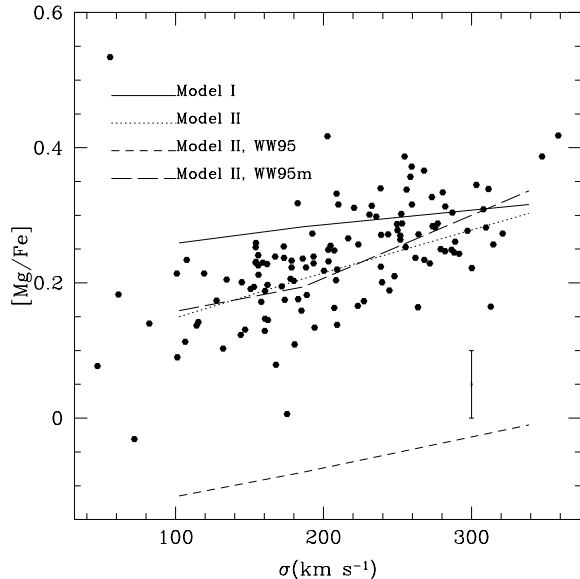


Figure 6. $[Mg/Fe]$ as a function of galactic velocity dispersion predicted by Model I (solid) and II (dotted) compared to the data from Gonzalez (1993), Mehlert et al. (2000), Beuing et al. (2002) converted to α/Fe ratios by Thomas, Maraston, & Bender (2002). The typical error is shown in the bottom-right corner. For comparison we show the theoretical curves obtained with the same input parameters of Model II, but different yields (see text). WW95: yields by Woosley & Weaver (1995). WW95m: yields by Woosley & Weaver (1995) modified according to François et al. (2003).

formed into $[\alpha/Fe]$ ratios by Thomas et al. (2002). It is clear that Model I does not predict the right slope for the $[Mg/Fe]$ - σ relation, and the results become worse if we use a smaller infall timescale. On the other side, Model II reproduces fairly well the observed relation, thus leading us to the conclusion that it can be chosen as the best one in our parameters space. With this choice we fixed the free parameters ν and τ in the nuclei of ellipticals. The other degrees of freedom, represented e.g. by a possible change of ν and τ with radius (see section 2.5 for the definition of the sub-models studied), will be constrained by the analysis of the radial gradients in metallicity and colors (sections 3.2 and 3.4, respectively).

Finally, we note that our results may be affected by the choice of the stellar yields. It is known that the yields by TNH give less iron (about 1/3 for massive stars) and slightly more Mg than the set computed by WW95, thus providing higher Mg/Fe ratios at a given metallicity (see also Thomas et al., 1999; Ferreras & Silk, 2002). We run our models also with WW95 yields and this implementation translates in the need of a shorter τ than those presented in Table 2 in order not to decrease the mean stellar $[Mg/Fe]$. When trying to evaluate the impact of the yields on the predicted line-strength indices, the situation is complicated by the adopted calibration. In particular, for the calibration based on Worthey's (1994) SSPs a shortening in τ would not necessarily imply a decrease in the central Mg_2 and $< Fe >$, since they are functions of the Fe abundance alone, which increases faster when WW95 yields are adopted.

In order to have a more quantitative picture, we show in Table 4 the indices and the mean stellar $[Mg/Fe]$ ratios pre-

dicted by our best model when different yields compilations are chosen. In column 1 the model is indicated; in columns 2 and 3 we present the adopted yields compilation and the assumed infall timescale, respectively, whereas in column 4 we show the time at which the galactic wind occurs. In columns 5 to 8 we show the indices predicted by means of either the Tantalo et al. (T) or the Worthey SSP (W); the last column shows the predicted stellar $\langle Mg/Fe \rangle$. As anticipated, the compilation of yields by WW95 translates in the need of very short infall timescale, in order to match the observed Mg overabundance. In particular, we have to increase ν from 10 Gyr^{-1} to 20 Gyr^{-1} or more, in order to obtain $\langle Mg/Fe \rangle > 0.1$. This result is reinforced by the last row of Table 4, where we show the predictions based on Pipino et al.'s (2002) best model. This particular model included WW95 yields and did not assume any initial gas flow and predicted reasonable values for the central metallicity indices as well as for the the mean stellar $[Mg/Fe]$.

On the other hand, it is worth noting that the use of WW95m set of yields gives the same results (within a few percent) obtained with our Model II with TNH96. These findings are also confirmed for the $10^{10} M_{\odot}$ and $10^{12} M_{\odot}$ galaxies, as one can see from Figure 6 (dashed and long-dashed curves for WW95 and WW95m cases, respectively). In conclusion, we underline the need for an initial infall episode, which allows us not only to build more realistic models, but also to match simultaneously the metallicity indices and the Mg overabundance in the core of bright ellipticals. As one can deduce from Table 6, our predictions for the central Mg_2 and $\langle Fe \rangle$ are robust and independent from the adopted yields compilation. The predictions for $[Mg/Fe]$ based on the best set of yields available are in reasonable agreement with the observed ones only when the infall term is present in the equation for the chemical evolution.

In concluding this section we want to stress that the diagrams presented in Figs. 4 and 6 represent powerful and independent tests for our models. In fact, in order to have high central indices, we need a long star formation period to obtain a suitable chemical enrichment; on the contrary, high values of $[Mg/Fe]$ require very short star formation timescales. To give an example, to produce a better agreement between the predicted curve and the observations in Fig. 6, we should increase ν (or decrease τ), but this produces lower values for Mg_2 and $\langle Fe \rangle$.

3.2 Metallicity gradients inside the galaxies

Once we have defined the influence of the total initial mass of the objects in determining the parameters which regulate galactic evolution, we intend to investigate the variation of the star formation and gas accretion histories among different regions of the same galaxy. In order to extract information on the mechanism of galaxy formation, we make use of the radial gradients in line-strength indices and colors as measured in ellipticals. In this section we focus on the variation of metallicity as a function of the galactocentric distance, whereas in section 3.4 we study the color gradients.

Metallicity gradients are observed in the stellar populations inside ellipticals (e.g. Carollo et al., 1993; Davies et al., 1993; Trager et al., 2000a). They can arise as a consequence of a more prolonged star formation, and thus stronger chem-

ical enrichment, in the inner zones. In the galactic core, in fact, the potential well is deeper and the wind develops later relative to the most external regions (e.g. Martinelli et al., 1998). From an observational point of view, however, the situation is not very clear. In fact, Davies et al. (1993) did not find any correlation linking the gradients to the mass or the $(Mg_2)_0$ of the galaxies, whereas Carollo et al. (1993) claimed a bimodal trend with mass, in which the Mg_2 gradient becomes flatter in high mass ellipticals. On the other hand, Gonzalez & Gorgas (1996) found that the gradient correlates better with $(Mg_2)_0$ than with any other global parameter. Recently, Kobayashi & Arimoto (1999) analysed a compilation of data in the literature, finding that the metallicity gradients do not correlate with any physical property of the galaxies, including central indices and velocity dispersion, as well as mass and B magnitude.

In what follows we present only the results for Model II, which seems to be the best in reproducing the mass-metallicity relation and the Mg enhancement, and we try to discriminate among the different sub-models (for their definition see section 2.5 and Table 5). In particular, we study a galaxy of $10^{11} M_{\odot}$ luminous mass by means of Model IIb, which assumes a τ decreasing from the 0.4 Gyr in the inner zone, to 0.01 Gyr at $R = R_{eff}$, whereas in Model IIc we adopted $\tau = 0.5$ Gyr at the effective radius. A summary of the sub-model properties for three particular shells (in order to sample the core, the $R \simeq R_{eff}/2$ zone and the $R \simeq R_{eff}$ region, respectively) of a $10^{11} M_{\odot}$ galaxy, is given in Table 5. In column 1 both the internal and the external radius defining that particular shell are shown; in column 2 we present the infall timescale at that radius, whereas in column 3 we show the time at which the galactic wind occurs. In columns 4 to 7 we show the indices predicted by means of either the Tantalo et al. SSP (T) or the Worthey SSP (W); the last three columns present the predicted mean stellar $\langle Mg/Fe \rangle$, $\langle Mg/H \rangle$ and $\langle Fe/H \rangle$, respectively. However, conclusions similar to the results presented here can be drawn for galaxies in the whole mass range. We recall that the central zone is the same in all the sub-models, since it is constrained by the results on central indices and $[Mg/Fe]$.

We show our results for the predicted trend of Mg_2 as a function of radius in Fig. 7 for a $10^{11} M_{\odot}$ galaxy by means of Model IIa,b,c. All the observed galaxies, shown for comparison, have a measured mass of $\sim 10^{11} M_{\odot}$. Each sub-model is plotted in a different panel. In any case the curves obtained with the Worthey calibration seem to agree better with the observed slope. In the bottom-right panel of Fig. 7, we show the predicted $[Mg/H]$ abundance gradient as a function of radius for the different sub-models. It is worth noting (as evident also from the entries in Table 5) that the stellar $\langle Mg/H \rangle$ as a function of radius behaves in the same way in all the three sub-models, thus producing an identical gradient ($\frac{\Delta[Mg/H]}{\Delta \log r} = -0.06$) in all cases. On the other hand, the predicted Mg_2 versus radius appears different according to the assumed calibration (e.g. Worthey or Tantalo et al.), especially at large radii; the reason for this relies in the fact that the calibration relations introduce a dependence on the $[Mg/Fe]$ and $[Fe/H]$ (see Fig. 8). As it can be seen from Fig. 7, we obtain a reasonable fit to the data only with Model IIb and the Worthey calibration. In general our curves lie around the average value of Mg_2 at a given radius, but,

Table 4. Model II with different yields for massive stars

Model	Yields	τ (Gyr)	t_{gw} (Gyr)	Mg_2		$\langle Fe \rangle$		$\langle [Mg/Fe] \rangle$
				T	W	T	W	
II	TNH96	0.4	0.709	0.298	0.285	3.33	3.17	0.206
II	WW95	0.4	0.704	0.240	0.295	3.34	3.27	-0.08
II	WW95	0.1	0.564	0.264	0.289	3.32	3.21	0.04
II	WW95m	0.4	0.705	0.299	0.288	3.36	3.21	0.194
P2002	WW95	-	0.439	0.299	0.274	3.26	3.07	0.253

The values presented in this table are referred to the central ($0 \rightarrow 0.1R_{eff}$) zone for a $10^{11}M_{\odot}$ galaxy. The indices obtained with the Tantalo et al. (1998) SSP are labeled with T, whereas W refers to the Worthey (1994) SSP (see text). TNH96: yields by Thielemann et al. (1996). WW95: yields by Woosley & Weaver (1995). WW95m: yields by Woosley & Weaver (1995) modified according to François et al. (2003). P2002: results from Pipino et al. (2002) best model.

Table 5. Model II - Summary of sub-model properties

Sub-model/ zone	τ (Gyr)	t_{gw} (Gyr)	Mg_2		$\langle Fe \rangle$		[Mg/Fe]	[Mg/H]	[Fe/H]
			T	W	T	W			
a									
$0 - 0.1R_{eff}$	0.4	0.709	0.298	0.285	3.33	3.17	0.206	0.07	0.116
$0.4 - 0.5R_{eff}$	0.4	0.579	0.287	0.264	3.17	2.98	0.245	0.03	0.007
$0.9 - 1R_{eff}$	0.4	0.544	0.284	0.258	3.12	2.92	0.258	0.02	-0.03
b									
$0 - 0.1R_{eff}$	0.4	0.709	0.298	0.285	3.33	3.17	0.206	0.07	0.116
$0.4 - 0.5R_{eff}$	0.2	0.490	0.293	0.257	3.13	2.92	0.306	0.03	-0.03
$0.9 - 1R_{eff}$	0.01	0.308	0.317	0.236	3.04	2.72	0.532	0.02	-0.145
c									
$0 - 0.1R_{eff}$	0.4	0.709	0.298	0.285	3.33	3.17	0.206	0.07	0.116
$0.4 - 0.5R_{eff}$	0.45	0.594	0.287	0.266	3.18	2.99	0.236	0.03	0.014
$0.9 - 1R_{eff}$	0.5	0.569	0.283	0.260	3.13	2.94	0.242	0.02	-0.016

Assumed infall timescale and predicted chemical abundances and line-strength indices as a function of radius for a $10^{11}M_{\odot}$ Model II galaxy. The calibrations used for Mg_2 and $\langle Fe \rangle$ marked with T are derived from the Tantalo et al. (1998) SSPs, whereas those labeled with W are based on Worthey's (1994) SSPs, see section 3. The abundance ratios in the last three columns are averaged over the stellar populations.

from a visual inspection of Fig. 7, it seems that every model predicts flatter slopes than those deduced from the observational points, especially in the inner zones. However Mg_2 gradients exhibit high dispersion in their slopes and central values; therefore, in order to have more robust estimates, we face this issue in a statistical way at the end of this section.

The fast decrease of the [Fe/H] ratio with radius in Model IIb galaxy (see Table 5 and upper panel of Fig. 8) produces a strong Mg enhancement in the outer regions, which is responsible for the upturn in the predicted Mg_2 at $R \sim R_{eff}$ (solid curve in the top-left panel of Fig. 7) when the Tantalo et al. calibration is adopted. The reason for this unexpected behaviour, completely at variance with the observed trend, could reside in the adopted ranges for [Fe/H] and [Mg/Fe] in Matteucci et al. (1998), who provided a calibration law by adopting the SSPs of Tantalo et al. (1998a) for specific values of the [Mg/Fe] ratio. In particular, these SSPs are limited to [Mg/Fe]=+0.3 whereas our $10^{11}M_{\odot}$ Model IIb galaxy has [Mg/Fe]=+0.532 in its outermost zone. On the other hand, since Model IIb with Worthey calibration produces the best gradient among the whole set of sub-models, in the following we refer to this model as to the best one.

This choice is confirmed by the analysis of the $\langle Fe \rangle$

gradient (Fig. 8). The slope predicted by different sub-models is flatter at larger radii, when considering the Tantalo et al. calibration (lines labeled with T). Also in this case, Model IIb with Worthey's relation agrees better with the data. We note, however, that the results obtained with the different sub-models and the two calibrations are consistent with each other within $2 - 3\sigma$ (the typical uncertainty is shown on the left side of the Figure 8). In fact, observations show a large scatter and also a large range in slopes. In any case, our best model well reproduces the mean values of the observed gradients. In fact, Davies et al. (1993) mean slope for $\langle Fe \rangle$ gradient is -0.38 ± 0.26 , consistent with our predictions for a $\sim 10^{11}M_{\odot}$ Model IIb: - 0.29 and - 0.45 for the Tantalo et al. and Worthey calibrations, respectively. It is very important to compare these values with the real abundance gradients. From Table 5 we derive $\frac{\Delta[Fe/H]}{\Delta \log r} = -0.119, -0.261, -0.132$ for Model IIa, IIb and IIc, respectively. Model IIb shows a very steep gradient in Fe (see small panel of Figure 8), in good agreement with the mean metallicity gradient found by Kobayashi & Arimoto (1999) $\frac{\Delta[Fe/H]}{\Delta \log r} = -0.30 \pm 0.12$, and the results of Davies et al. (1993). A fundamental conclusion which can be drawn from the discussion presented above, is that, while the variations in Mg_2 depend on the radial gradients in [Fe/H] and

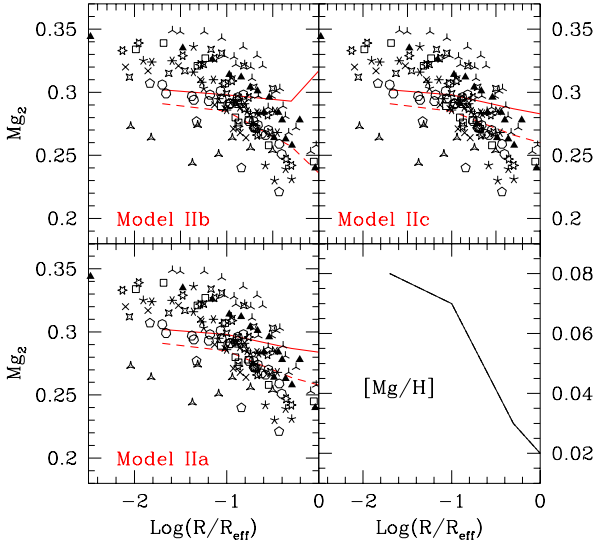


Figure 7. Mg_2 gradient predicted by different sub-models for a $\sim 10^{11} M_{\odot}$ galaxy compared with observations. Each symbol correspond to one galaxy from Carollo et al. (1993). Predictions for both Worthey (dashed line) and Tantaló et al. (solid line) calibration are plotted. The typical error for Mg_2 is $\sim 0.002\text{mag}$ in the innermost zone and $\sim 0.01\text{mag}$ at larger radii. In the bottom-right panel, the predicted $[Mg/H]$ abundance gradient is shown for the three sub-models (see text for details) and the same galactic mass.

$[Mg/Fe]$ (see Fig. 8), the predicted $\langle Fe \rangle$ gradient reflects instead the variation of the real abundance, $[Fe/H]$, as a function of galactic radius (see Fig. 8).

As a further step in our analysis, we followed the suggestion by Kobayashi & Arimoto (1999). In particular, we derived the slope and the intercepts of line-strength gradients via a least-square fit:

$$Mg_2(r_i) = (Mg_2)_{eff} + \frac{\Delta Mg_2}{\Delta \log r} \log \frac{r_i}{r_{eff}}, \quad (10)$$

where $Mg_2(r_i)$ is the index predicted in the i -th shell of radius r_i and the subscript eff means that the values are computed at the effective radius R_{eff} . The same procedure was carried out by Kobayashi & Arimoto (1999) for the observed gradients. To be consistent with the gradients obtained from the observations we limit our analysis to $0.1 R_{eff}$, since Kobayashi & Arimoto (1999) neglected data taken at inner radii to avoid seeing effects. We applied this procedure to galactic models in the $10^{10} - 10^{12} M_{\odot}$ mass range and our results are plotted in Fig. 9. With this kind of diagnostic we can check in a statistical way whether the predicted slopes match average value of the observed ones as a function of the galactic mass, in order to obtain a more quantitative comparison between our Model IIb and the observed gradients.

We tuned τ in order to obtain reasonable values for the indices in each zone. In particular, we fixed $\tau = 0.01$ Gyr at $R = R_{eff}$ for the models with initial masses of $\sim 10^{10} M_{\odot}$ (as found for the $\sim 10^{11} M_{\odot}$ case), and $\tau = 0.06$ Gyr for the most massive galaxies. From the bottom panel of Fig. 9 we note the excellent agreement with the average value of

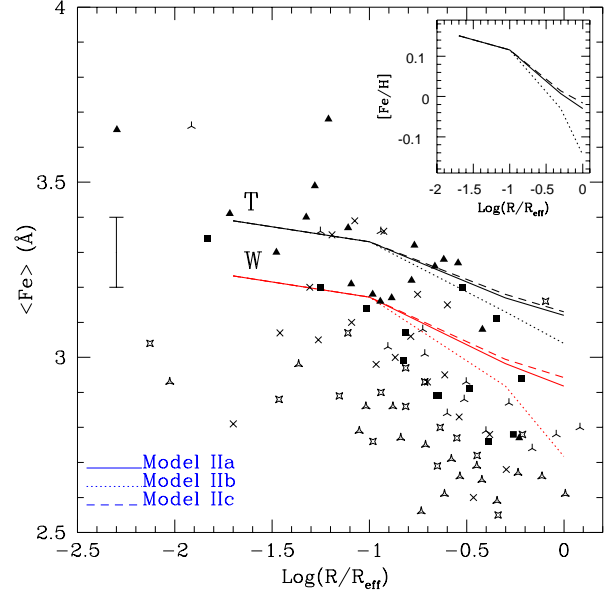


Figure 8. $\langle Fe \rangle$ gradient predicted by different sub-models for a $\sim 10^{11} M_{\odot}$ galaxy compared with observations. Each symbol corresponds to one galaxy from Davies et al. (1993) data. The predictions based on Worthey calibration are labeled with W , whereas those from Tantaló et al. with T . The typical error is shown on the left. In the small panel in the top-right corner we show the predicted $[Fe/H]$ as a function of radius for the same models.

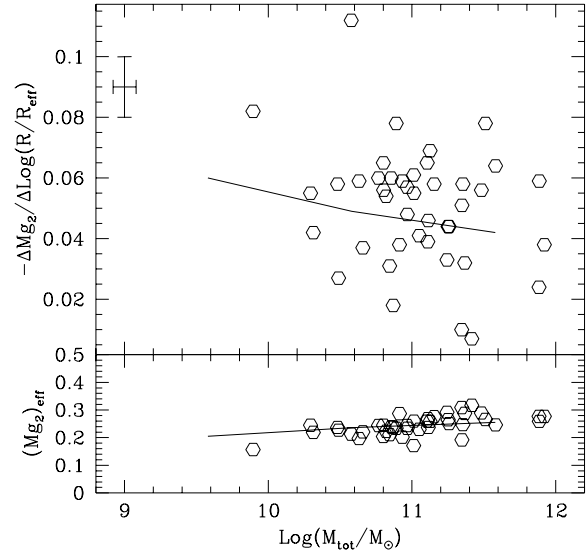


Figure 9. Mg_2 gradient slope and intercept defined as in eq. 10 from Model IIb. Data from Kobayashi & Arimoto (1999).

Mg_2 measured at the effective radius. Our model predicts a logarithmic slope for this index which is very close to the average observed gradient, although we obtain slightly flatter gradients for the most massive galaxies. This is a clear consequence of the adopted inverse wind scenario, in which the more massive galaxies form faster. In any case, this approach allows us to show the goodness of our models in a

clearer way than that presented in Fig. 7. The little disagreement with observations can be explained as a consequence of the predicted metallicity in the core of the most massive galaxies, which seems to be smaller than the observed one (at least for what can be deduced from the comparison made in Fig. 4). As evident from Figure 9, there is a large scatter in the observed slopes, but on the average $\frac{\Delta M_{g2}}{\Delta \log r}$ seems to be independent from the mass of the galaxies.

As in the case of the central indices, the combined analysis of M_{g2} and $\langle Fe \rangle$ variations along the galactic radius can provide a measure of the $[Mg/Fe]$ gradient. A reliable estimate of the slope of the $[Mg/Fe]$ gradient represents a very useful tool to discriminate between outside-in and inside-out formation scenarios. Our best model predicts $\frac{\Delta[Mg/Fe]}{\Delta \log r} = 0.326$ (in the case of a $\sim 10^{11} M_{\odot}$ galaxy), whereas model IIa and IIc seem to suggest flatter slopes. Hints for a positive slope in the most massive galaxies, in agreement with our predictions, can be found in the analysis made by Ferreras & Silk (2002) based on Trager et al. (2000a) data; however the scatter increases and the mean slope for a given galactic mass decreases if the Kobayashi & Arimoto (1999) compilation is added to the Trager et al. (2000a) points. On the other hand, in a very recent study of Coma early-type galaxies, Mehlert et al. (2003) claimed that, on average, these galaxies do not exhibit gradients in α/Fe , thus disfavoring models with strong inside-out or outside-in formation scenarios. Given the importance of the topic, larger compilations of homogeneous data are required before considering this issue completely solved.

3.3 Color-Magnitude relation

In the following sections we focus on the photometric results, in order to show how the good agreement achieved between Model IIb and the abundance patterns translates into a fit of the observed colors. In order to do that, we followed the standard route in the context of the monolithic collapse, namely the CMR arises directly from the mass-metallicity relation (i.e. stellar populations with higher metal content show redder colors). Moreover, the very small scatter observed in the colors as a function of the total V magnitude for galaxies in Virgo and Coma clusters (Bower et al., 1992), and the fact that it is observed in different environments and at different redshift (e.g. Stanford et al., 1998; Bernardi et al., 2003) are interpreted as evidences of an highly synchronized epoch of elliptical formation at high redshift (Bower et al., 1992; Renzini & Cimatti, 1999). However, from a theoretical point of view, the well-known age-metallicity degeneracy implies that the presence of a significant fraction of younger (i.e. bluer) stellar populations can be masked if they have a high metal content. This kind of age-metallicity conspiracy has been claimed by several authors (e.g. Trager et al., 1998, 2000; Ferreras et al., 1999; Jorgensen, 1999, but see Kuntschner, 2000, and Kuntschner et al., 2001, for a different point of view) in order to reconcile the tightness of the CMR with evolutionary model in which the star formation continues until low redshifts, as a consequence of late mergers. The question is still under debate and we intend to assess this issue separately in a forthcoming paper. Therefore, we assume our galaxies to form simultaneously at high redshift. We recall that the epoch of galaxy formation adopted in this paper is $z_f = 5$ (i.e. our model ellipticals are 12.3 Gyr old).

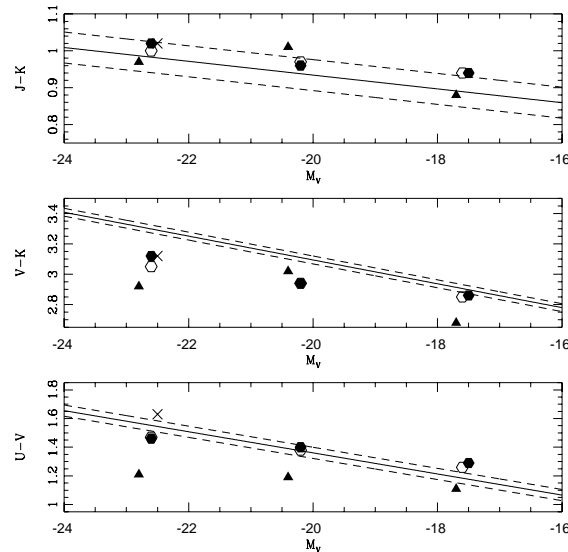


Figure 10. Predicted CMRs for Model I (empty hexagons), Model II (full hexagons) and the best model by Pipino et al. (2002, triangles). The solid lines represents the fits of Bower et al. (1992b) data, with their 1σ scatter (dashed lines). The prediction from the model with fixed metallicity ($Z=0.03$, see text) is shown by a cross.

In a future paper we shall analyse galactic models in which alternative scenarios of galaxy formation will be assumed. In particular we intend to test the possible role of merging, late episodes of gas accretion, secondary bursts of star formation in the CMR and the chemistry of ellipticals.

Before presenting the photometric results, we recall that Jimenez et al. (1998) photometric code was applied to the SSPs predicted by our models, thus taking into account in a self-consistent way the chemical evolution of the ISM.

Fig. 10 shows the predicted Color-Magnitude relations for U-V, V-K and J-K colors (Model I and II) versus total V magnitude compared to the observed data which are represented by their best fit (Bower et al., 1992b; solid lines). The predicted colors are obtained by adding the different shells contributions up to ~ 5 kpc from the galactic center, whereas the total M_V is relative to the whole galaxy (up to $10 R_{eff}$), in order to be consistent with Bower et al. (1992a), who obtained their data on colors with a fixed aperture of $5h^{-1}$ kpc, whereas, for the V magnitude, they used its *total* value (see Kawata, 2001, for a detailed discussion). This procedure becomes necessary for a sampling of the central regions in the high mass models, since it simulates the observed aperture and it can be done simply by avoiding the inclusion of the most external parts, where the presence of the color gradients would make the predicted colors bluer. Model I and II agree very well with the data in the J-K and U-V versus M_V diagrams. We note a slightly flatter trend for our curves relative to the data, but still consistent within the scatter (~ 0.04 mag, Bower et al. 1992b, dashed lines in Fig. 10) of the observed galaxies around the mean relation. We recall that also the slopes obtained from the fit to the data have their own error of 0.01 (see Bower et al. 1992b). For comparison, we plot also the CMR predicted

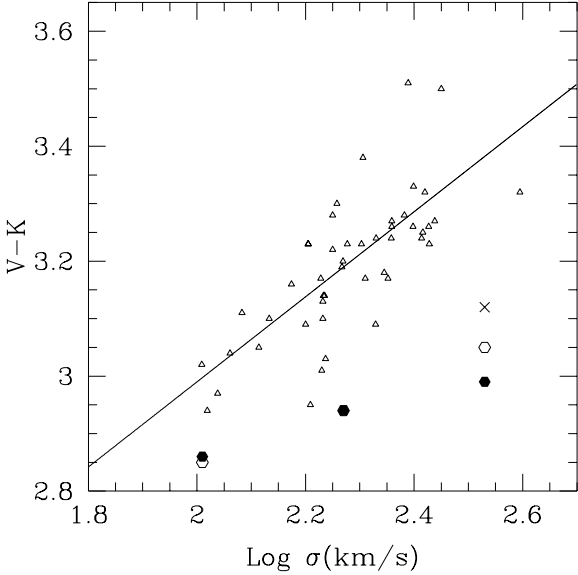


Figure 11. Predicted V-K versus velocity dispersion for Model I (empty hexagons) and II (full hexagons) compared to the data from Mobasher et al. (1999, triangles). The line represent the fit of the data. The prediction from a model with fixed metallicity ($Z=0.03$, see text) is shown by a cross.

by Pipino et al. (2002) best model (triangles). In spite of the fact that this model is very similar to the ones presented in this paper, it does not consider infall, thus it produces a larger fraction of stars formed from low-metallicity gas than our Model II. Consequently, the lower mean metallicity predicted for the stellar populations in the best model of Pipino et al. (2002) makes the galactic light bluer. We do not show Model III results, since they fail in reproducing the CMR (e.g. $V - K \sim 3.7$ for the more massive galaxies) due to a too high mean stellar metallicity.

On the other hand, our model predictions fail in reproducing the right slope for V-K versus M_V . In particular, we found a V-K which is about 0.5 mag less than the observed one for the most massive galaxies. This problem becomes more evident in Fig. 11, where we plot the color as a function of the galactic velocity dispersion. However, we consider this particular plot less constraining than the color- M_V diagram, since the predicted relation could be systematically biased by the relation adopted to convert the total magnitude of the object into the observed σ . Several authors in the literature (e.g. Arimoto & Yoshii, 1987; Romano et al., 2002) pointed out that, since the V-K color has a strong dependence on the global metallicities, models with Salpeter IMF hardly match the observed CMR, producing in general bluer galaxies. On the other hand, the fact that the V - K predicted by the best model of Pipino et al. (2002, with inverse wind but without infall) flattens at high luminosities, reinforces the conclusion that the disagreement is caused by a too low predicted metallicity for the cores of the most massive ellipticals with respect to observations, and not by the presence of the initial infall episode. We tried to reconcile our predictions with the data by varying *ad hoc* the mean stellar metallicity ($\langle Z \rangle$), while we kept fixed the IMF and the star formation history for the $10^{12}M_{\odot}$ Model II galaxy. In Table 6 we show the

Table 6. The effect of metallicity on colors.

$\langle Z \rangle$	M_V	L_B ($10^{10}L_{\odot}$)	L_K ($10^{10}L_{\odot}$)	U-V	V-K	J-K
0.02	-22.7	7.78	40.5	1.49	3.03	0.99
0.03	-22.5	6.29	41.2	1.63	3.12	1.02
0.04	-22.3	4.80	41.9	1.76	3.39	1.10
0.10	-21.8	2.93	47.6	2.30	3.34	1.26
Model II	-22.6	7.42	40.6	1.46	3.04	1.00
Model BC	-22.2	5.49	26.9	1.41	3.02	0.87

Luminosities and colors predicted by a $10^{12}M_{\odot}$ galaxy of Model II, compared to models with fixed metallicity, but same star formation history. Model BC: Model II colors predicted by means of Bruzual & Charlot (1993) code with solar metallicity.

colors obtained with several fixed metallicities compared to our case (Model Iib) which predicts $\langle Z \rangle = 0.025$. Since the differences in the stellar evolution prescriptions included in the photometric codes could generate 0.25 mag discrepancies in V-K (Charlot et al., 1996), we checked our finding by comparing it with the results obtained with the Bruzual & Charlot (1993) code with solar metallicity, applied to our Model II. As it can be seen from the last row of Table 6, also in this case the predictions do not agree with the observed values. We reject the high metallicity models, which predict redder colors than the typical values of the observed CMR (see the entries in Table 6) for a given M_V . On the other hand, the $\langle Z \rangle = 0.02$ model predictions are very similar to our 'self-consistent' case, as expected, since they have nearly the same metallicity. The model with $\langle Z \rangle = 0.03$ (cross in Figs. 10 and 11) gives a better fit for the V-K - M_V relation, but makes the agreement slightly worse for the other two colors. In conclusion, in order to have a good fit to the three CMRs, it is necessary to increase the mean stellar metallicity from $\langle Z \rangle = 0.025$ to $\langle Z \rangle = 0.035$ at most. This can be obtained by assuming a slightly flatter IMF with exponent $x=1.25$, which gives $Mg_2 = 0.312$ mag, $\langle Fe \rangle = 3.42 \text{ \AA}$ and $[Mg/Fe] = 0.341$ dex in the central zone (still consistent with observations) and $\langle Z \rangle = 0.037$ within the inner 5 kpc.

3.4 Color gradients

The analysis of the color gradients in the stellar populations of elliptical galaxies can reinforce the results found in the previous sections. It is, in fact, observed (e.g. Peletier et al. 1990) that stars in the galaxy centers are redder than those in the outer regions, and colors become progressively bluer with increasing radius. Also in this case, the variation of the gradient strength as a function of redshift seems to be consistent with passive evolution (Saglia et al., 2000). The analysis of these gradients out to redshift ~ 1 led Tamura et al. (2000) to the conclusion that they originate mainly from the variations in the mean stellar metallicity rather than from an age sequence. Following the same procedure adopted in section 3.2 to compare the predicted metallicity gradients with observations, we show in Figs. 12 and 13 the slopes and the intercepts at $R = R_{eff}/2$ for U-R and B-R color gradients as predicted by Model Iib and compared with the data from Peletier et al. (1990).

As expected from the good agreement between our mod-

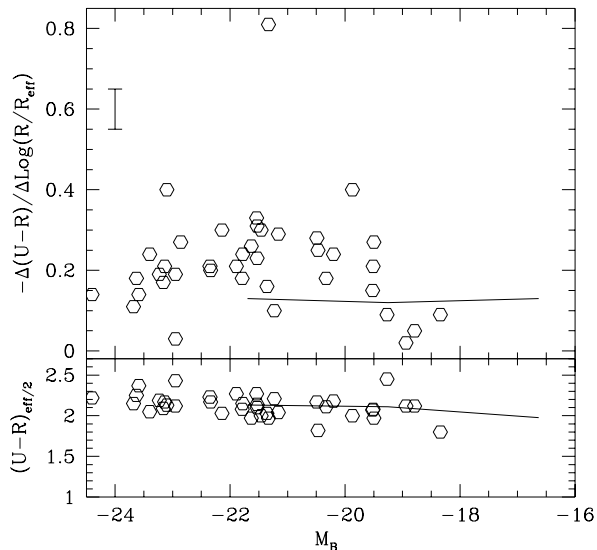


Figure 12. Predicted U-R color gradient as a function of galactic total M_B for Model IIb compared with the data from Peletier et al. (1990).

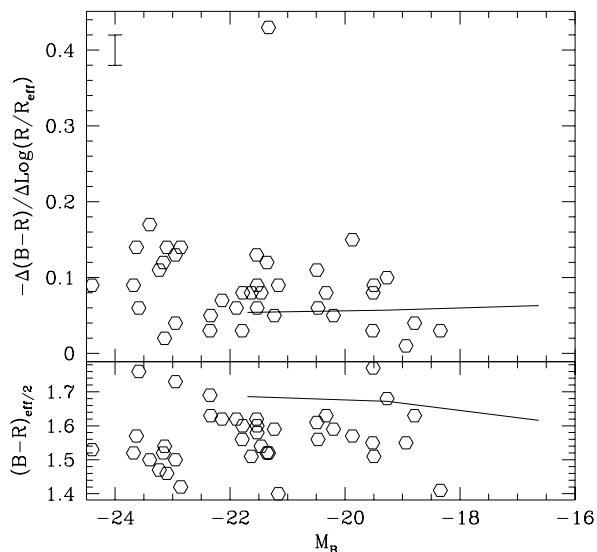


Figure 13. Predicted B-R color gradient as a function of galactic total M_B for Model IIb compared with the data from Peletier et al. (1990).

els and the line-strength gradients, we note from the figures that the predicted intercepts at $R = R_{eff}/2$, as well as the slopes, are pretty close to the average value of the observed ones. With the help of this diagnostic we can rule out the sub-model c with $\tau < 0.2$ Gyr in the inner zone, since it produces positive color gradients due to the presence of galactic winds which start earlier in the core than in the outskirts of a galaxy. Therefore, we can rule out inside-out mechanisms for the formation of elliptical galaxies similar to those invoked for spiral discs (e.g. Matteucci & François, 1989; Chiappini

et al., 1997), in which a strong (i.e. $\Delta\tau \gg 1$ Gyr) variation in τ between the innermost and the outermost regions is assumed. In this case, the timescale for the infall is increasing with galactic radius, inducing the external regions to evolve much more slowly than the internal ones. A large variation in age between the inner and the outer stellar populations seems to be ruled out also by the recent results of Mehlert et al. (2003, see also Sec 3.2).

It is worth noting that Menanteau et al. (2001a) showed that a fraction of field early-type galaxies exhibit blue cores. The properties of these galaxies can be reproduced by means of Martinelli et al. (1998) multizone model, which is an outside-in formation model as the one presented here, and by assuming that only $\sim 20\%$ of the galaxies have been formed very recently (Menanteau et al., 2001b), being the blue color of the central region of the galaxies associated to more prolonged star formation in the core with respect to the outskirts. Moreover, it is well known that field ellipticals as a whole are $\sim 1 - 2$ Gyr younger than the counterpart living in clusters (e.g. Bernardi et al., 1998). The presence of a late episode of star formation in the galactic core can be explained in terms of accretion/merging events or by a residual star formation which survived the development of the galactic wind in the very center of the galaxy.

3.5 Mass to light ratio

In this last section we deal with the fundamental plane and, in particular, we focus on the possible variation of the mass-to-light ratio as a function of the mass of the galaxy (FP seen *edge-on*). We recall that if ellipticals were a perfect homologous family, the FP could be explained by means of the virial theorem (e.g. Renzini & Ciotti, 1983). The difference from the expected relation in the plane seen edge-on is called the *tilt* of the FP. The FP edge-on is simply the projection of the locus in which ellipticals lie on the plane formed by the two parameters κ_1 and κ_3 linked to the mass and to the mass-to-light ratio (M/L), respectively (see Bender et al., 1992; Burstein et al., 1997). Therefore the observed tilt translates into a systematic variation of the M/L with the mass or the luminosity.

Our results in the B and K-band are plotted in Fig. 14, where the solid line represents the fit to Mobasher et al. (1997) data in the near-infrared, and the dashed line the fit to Burstein et al. (1997) data in the B-band derived at the effective radius. The predicted luminosities for our galaxies are given in Tables 1 and 2, whereas the *stellar* masses adopted in deriving the mass-to-light ratio are $\sim 20 - 30\%$ of the nominal mass. In both bands our models exhibit a flat behaviour at odds with observations, and this is because we assume a constant IMF. However the average theoretical M/L_B values are close to the observed ones, whereas the M/L_K values suffer from the effects of the too low L_K predicted by our models. In fact, since we are using the stellar mass, i.e. neglecting the contribution of the dark matter, the only solution (at fixed IMF) in order to match the observed M/L_K is to increase the K-band luminosity. In order to solve this discrepancy, one possibility could be a change in the mean stellar metallicity of the same factor we need to match the V-K color in high mass ellipticals. By using the B-luminosities displayed in Table 6, we infer an increase in $\log(M/L_B)$ of the order of $\sim 0.1 - 0.2$ for a $< Z \geq 0.035$

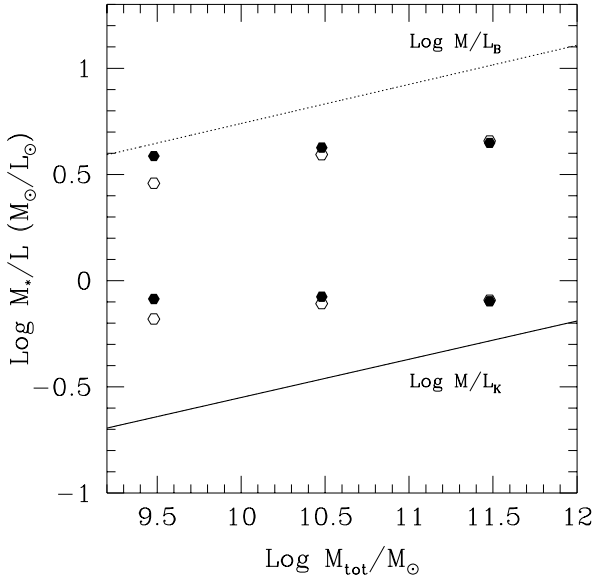


Figure 14. Predicted M/L in B- and K-band for Model I (empty hexagons) and Model II (full hexagons) as a function of the galactic mass. Solid line: fit from Mobasher et al. (1997) data in the near-infrared. Dashed line: fit from Burstein et al. (1997) for the B-band.

model. If this change is applied only to the most massive galaxy, it could help in reproducing the right slope.

A solution often invoked to explain the tilt of the FP is a change in the IMF, which has to become flatter with increasing initial mass (e.g. Renzini & Ciotti, 1993; Matteucci, 1994). In this case we still have a change in metallicity, but also a decrease in the low-mass stars contributing to the mass observed at the present time. If we consider a case in which the $10^{10} M_{\odot}$ galaxy of Model II has a Salpeter IMF and the $10^{12} M_{\odot}$ galaxy an AY one, we obtain a M/L_B ratio increasing of about a factor of 1.3, with a slope which becomes steeper and similar to the observed one. On the other hand, the $\log(M/L_K)$ decreases to the value of -0.32, thus reaching the observed relation, but producing a decreasing trend in $\log(M/L_K)$ as a function of mass, completely at variance with the solid line in Fig. 14. In any case, such kind of model would fail in reproducing the CMR (see section 3.3), and the Mg_2 -mass relation (with $(Mg_2)_0 > 0.35 mag$ for the most massive galaxies). We also tried the intermediate IMF used in section 3.3.

However, recent results from Scodreggio et al. (1998) seem to question the tilt of the FP, at least in the near infrared. After correcting for the completeness, they found $M/L_B \propto L_B^{0.18}$ and $M/L_K \propto L_K^{0.08}$. Furthermore they claim zero tilt in the K-band in case of fully corrected samples. In this case the increasing slope of the mass-to-light ratio for bluer bands is driven by the CMR. Finally, other possible solutions to the tilt of the FP not investigated in the present paper, invoke e.g. deviation from homology (e.g. Busarello et al., 1997), or changes in the DM content as a function of luminous mass (see Ciotti & Renzini, 1993).

4 DISCUSSION AND CONCLUSIONS

In this paper we have demonstrated how the majority of the observables in ellipticals can be reproduced within a reasonable agreement by using a multizone model for the photochemical evolution of elliptical galaxies based on the standard collapse of a gas cloud on short timescales occurring at high redshift. In particular, we fixed the free parameters in our best model (namely the collapse timescale τ and the efficiency of star formation ν), by requiring that they can reproduce the mass-metallicity and the color-magnitude relations, as well as the Mg enhancement in massive galaxies and the metallicity gradients. After a detailed analysis, we ruled out models with a flat IMF ($x=0.95$, Model III) or with infall timescale constant with galactic mass (Model I). Our best model has a Salpeter IMF, a star formation efficiency increasing with galactic mass and a shorter infall timescale for the most massive objects.

Before concluding, we discuss here some of the assumptions made in this paper and their consequences for the theory of galaxy formation and evolution.

First of all, we focus on the relative weights that the star formation efficiency and infall timescale have in driving the mass-metallicity relation. In particular, our assumptions on τ and ν can be discussed in the light of previous results. This issue, in fact, has been recently investigated also by Ferreras & Silk (2003). With the help of a simple model of star formation they explore the correlation between U-V colour and $[Mg/Fe]$ ratios and conclude that a scenario where $\nu \propto M_{lum}$ should be favoured. Thomas et al. (2002) favour also a similar model, in which the more massive objects formed stars at very high redshift, with a typical duration of the star formation of ~ 0.5 Gyr, whereas less massive galaxies could exhibit star formation even at $z < 1$. Moreover, Ferreras & Silk (2003) conclude that the effects of ν and τ are degenerate, so they can be at work together, in a scenario in which $\tau \propto 1/\sqrt{M_{lum}}$. An infall timescale decreasing with galactic mass can be physically motivated on the basis of the following arguments. First of all, in a galactic formation scenario in which the galaxies are assembled starting from gas clouds falling onto the galactic potential well, the more massive objects have a higher probability (i.e. a higher cross section) to capture the clouds than the less massive ones, thus completing their assembly in a faster timescale (Ferreras & Silk, 2003). This picture is consistent with the other fundamental hypothesis of this paper, namely that ν increases with the galactic mass. In fact, the inverse wind picture can be explained by higher densities or higher cloud-cloud collision velocities in more massive ellipticals, determined by the assembly of these galaxies by means of the merging of gaseous protoclusters (Matteucci, 1994). Moreover, as a consequence of the more intense star formation, the more massive galaxies experience a stronger SN feedback with respect to the less massive ones. Therefore, the gas in the hot phase is able to halt the cold infalling gas earlier in a $10^{12} M_{\odot}$ model than in a $10^{10} M_{\odot}$ galaxy, thus making shorter the accretion timescale of the former with respect to the latter.

This is in contrast with the belief that the infall timescale should be proportional to the free-fall time, as suggested by several authors (e.g. Tantaló et al. 1998b, Romano et al. 2002). In fact, Tantaló et al. (1998b) assumed τ to be an increasing function of the galactic mass, while their

ν increases with decreasing galactic mass and, within the same model, going towards larger radii. This is necessary, in their model, to create metallicity gradients inside the galaxies. In fact, although the physical meaning of this choice is not clear, the increase in star formation efficiency with radius counter-balances the increase in the infall timescale and preserves the metallicity gradient. We did not explore this possibility, since an increasing ν with galactocentric radius would mean that the star formation is more efficient where the gas density is lower, at variance with observations and with the concept of the 'inverse wind'.

On the other hand, Romano et al. (2002) avoided this problem by assuming that the star formation has a shorter duration in more massive systems due to the appearance of a quasar phase, occurring first in the most massive systems.

Finally, in a recent paper, Kawata & Gibson (2003) supported the conclusion that τ should increase with the galactic mass by means of chemodynamical simulations. They found that radiative cooling becomes more efficient and thus the gas infall rate increases with decreasing galactic mass. However, they did not reproduce the $[\text{Mg}/\text{Fe}]$ increasing with galactic mass, since they did not assume ν increasing with mass.

In conclusion, the $\tau - M_{lum}$ relation we found could seem counter-intuitive in explaining the mass-metallicity relation, particularly if we see the problem under a classic-wind-perspective. Nevertheless, we underline that despite of the shorter star forming period, more massive models have a more efficient star formation (in our models it could be about an order of magnitude higher, see Tables 1, 2 and 3) and, thus, a faster metal production which can produce the correct mass-metallicity relations and CMRs.

Only when we compare our predictions for line-strength indices and colors for the $10^{12}M_{\odot}$ case, we obtain a too low predicted mean stellar metallicity. The very short star formation timescale, constrained by the $[\text{Mg}/\text{Fe}]$ ratio, does not allow the galaxies to reach high values for the central Mg_2 , and this could be a limit of the inverse wind picture; however, we recall that these conclusions may depend on the assumed index calibration (see section 3.2) and on the adopted yields (see section 3.1.2), once the IMF has been specified.

A possible way of solving the problem of the too low central metallicity predicted in the core of massive ellipticals is perhaps suggested by our best model. Since we showed that a model with the infall timescale decreasing with radius is the best one in reproducing the observed gradients in ellipticals, we can imagine a scenario in which a galaxy forms very fast in its external parts, while the inner regions are still accreting gas and forming stars. In other words, this resembles to the scenario proposed by Larson (1974) for the formation of ellipticals. In this scenario, the first stars form all over the original collapsing gas cloud and while the stars remain where they formed, the residual gas keeps collapsing towards the center. In this picture, the gas enriched in metals from the first stellar generations accumulates in the galactic center where the star formation lasts longer. In our model, the star formation is then inhibited first in the outskirts of the galaxies and later in the inner regions, owing to the heating of the ISM and consequent galactic wind. However, we do not consider the possible radial flows connected to the collapsing gas which settles towards the center. This mech-

anism could reconcile our predictions for the central indices with the observations and provide a natural explanation for our findings.

Another possibility for obtaining a higher central metallicity, could be a slightly flatter IMF in more massive galaxies. As we infer from the analysis of the CMR (Sec. 3.3) and of the M/L (Sec. 3.5) an exponent $x=1.25$ could be the case for a $10^{12}M_{\odot}$ model.

Our main conclusions can be summarized as follows:

(i) Starting from a fast assembly of gaseous clouds at high redshift, we obtain ~ 12 Gyr old galaxies, suffering a galactic wind at early times ($t_{gw} \leq 1.3$ Gyr) and undergoing passive evolution since then, whose properties match very well many observations. In particular, our best model reproduces the Mg and Fe abundances in the cores as well as the Mg overabundance relative to Fe, as inferred from the analysis of the line-strength indices. The multi-zone formalism allows us to predict the variation of these abundances and abundance ratios with radius. We predict abundance gradients in good agreement with observations, once a transformation of abundances into indices is made. Furthermore we find that the observed Ca underabundance relative to Mg can be real, due to the non-negligible contribution of type Ia SN to the production of this element.

(ii) In the framework of the 'inverse wind' model we suggest that the most massive ellipticals formed stars for a shorter period than less massive ones. This mechanism implies that the most massive objects are older than the less massive ones, in the sense that larger galaxies undergo passive evolution at earlier times. As a consequence of this and the different roles played by type Ia and II SNe, we are able to reproduce the observed increase of the average stellar $[< Mg/Fe >]$ with galactic mass (e.g. central velocity dispersion).

(iii) The photometric properties such as the color-magnitude relation and the color gradients have a natural explanation as due to variations in metallicity.

(iv) The Salpeter (1955) IMF seems to be the best one in order to reproduce the mean photo-chemical properties of elliptical galaxies. We recall here that models with the Salpeter IMF are also successful in reproducing the metals and the energy of the intracluster medium (Pipino et al., 2002) as well as the chemical abundances in Lyman-break galaxies (Matteucci & Pipino, 2002). Only in high mass models a slightly flatter IMF seems to be required to match the observed Color-Magnitude relation.

(v) The initial infall episode seems to be necessary to explain the observed $[\text{Mg}/\text{Fe}] \sim 0.1 - 0.4$ dex in the central cores of elliptical galaxies. In fact, closed-box models would predict, for the same stellar yields, too high values for the $[\text{Mg}/\text{Fe}]$ ratio. Furthermore, since the gas accretion modulates the star formation rate, the galactic wind and the ISM enrichment history are strongly influenced by the infall. Therefore, in our models, the initial accretion episode represents one of the main drivers of the mass-metallicity relations.

(vi) Elliptical galaxies have probably formed outside-in, i.e. the most external regions are older and stop forming stars before the central ones, a suggestion which needs to be tested with detailed chemo-dynamical models.

ACKNOWLEDGMENTS

We are indebted with R. Jimenez for providing his photometric code, and to D. Thomas for his data on [Mg/Fe]. We thank the anonymous referee for his careful reading of the paper. Finally we wish to thank F. Calura and C. Chiappini for interesting discussions.

REFERENCES

- Anders, E., & Grevesse, N., 1989, *Geochim. Cosmochim. Acta*, 53, 197
- Arimoto, N., & Yoshii, Y. 1987, *A&A*, 173, 23 (AY)
- Bekki, K., & Shioya, Y. 1999, *ApJ*, 513, 108
- Bender, R., Burstein, D., & Faber, S.M. 1992, *ApJ*, 399, 462
- Bernardi, M., Renzini, A., da Costa, L.N., Wegner, G., Alonso, M.V., Pellegrini, P.S., Rit e, C., & Willmer, C.N.A. 1998, *ApJ*, 508, L143
- Bernardi, M., Sheth, R.K., Annis, J., et al. 2003, *AJ*, 125, 1882
- Bertin, G., Saglia, R.P., Stiavelli, M., 1992, *ApJ*, 384, 423
- Beuing, J., Bender, R., Mendes de Oliveira, C., Thomas, D., Maraston, C., 2002, *A&A*, 395, 431
- Bower, R.G., Lucey, J.R., Ellis, R.S., 1992a, *MNRAS*, 254, 589
- Bower, R.G., Lucey, J.R., Ellis, R.S., 1992b, *MNRAS*, 254, 601
- Bressan, A., Chiosi, C., Fagotto, F. 1994, *ApJs*, 94, 63
- Bruzual, G., & Charlot, S. 1993, *ApJ*, 405, 538
- Butcher, H.R., & Oemler, A. 1978, *ApJ*, 219, 18
- Burstein, D., Bender, R., Faber, S.M., & Nolthenius, R. 1997, *AJ*, 114, 1365
- Busarello, G., Capaccioli, M., Capozziello, S., Longo, G., & Puddu, E. 1997, *A&A*, 320, 415
- Cappellaro, E., Evans, R., Turatto, M., *A&A*, 1999, 351, 459
- Carollo, C.M., Danziger, I.J., & Buson, L. 1993, *MNRAS*, 265, 553
- Cioffi, D.F., McKee, C.F., & Bertschinger, E., 1988, *ApJ*, 334, 252
- Charlot, S., Worthey, G., Bressan, A. 1996, *ApJ*, 457, 625
- Chiappini, C., Matteucci, F., Gratton, R. 1997, *ApJ*, 477, 765
- Chiosi, C., & Carraro, G. 2002, *MNRAS*, 335, 335
- Colless, M., Burstein, D., Davies, R.L., McMahan, R.K.Jr, Saglia, R.P., Wegner, G. 1999, *MNRAS*, 303, 813
- Daddi, E., Cimatti, A., Pozzetti, L., Hoekstra, H. Roettgering, H.J.A., Renzini, A., Zamorani, G., Mannucci, F. 2000, *A&A*, 361, 535
- Davies, R.L., Sadler, E.M., & Peletier, R.F., 1993, *MNRAS*, 262, 650
- de Freitas Pacheco, J.A., Michard, R., Mohayaee, R. 2003, *astro-ph/0301248*
- Djorgovski, S., & Davis, M. 1987, *ApJ*, 313, 59
- Dressler, A., Lynden-Bell, D., Burstein, D., Davies, R.L., Faber, S.M., Terlevich, R.J., & Wegner, G. 1987, *ApJ*, 313, 42
- Dressler, A., Oemler, A., Couch, W.J., Smail, I., Ellis, R.S., Barger, A., Butcher, H., Poggianti, B.M., & Sharples, R.M. 1997, *ApJ*, 490, 577
- Ellis, R.S., Smail, I., Dressler, A., Couch, W.J., Oemler, A.Jr., Butcher, H., & Sharples, R.M., 1997, *ApJ*, 483, 582
- Faber, S.M., Burstein, D., & Dressler, A. 1977, *AJ*, 82, 941
- Faber, S.M., Worthey, G., & Gonzalez, J.J. 1992, in *IAU Symp.* n.149, eds. B. Barbuy & A. Renzini, p. 255
- Ferreras, I., Charlot, S., & Silk, J. 1999, *ApJ*, 521, 81
- Ferreras, I., & Silk, J. 2002, *MNRAS*, 336, 1181
- Ferreras, I., & Silk, J. 2003, *MNRAS*, 344, 455
- Fran ois, P., Matteucci, F., Cayrel, R., Spite, M., Spite, F., & Chiappini, C. 2003, submitted to *A&A*
- Gonzalez, J.J., 1993, PhD thesis, Univ. of California
- Gonzalez, J.J., & Gorgas, J. 1996, in *ASP Conference Series*, 86, Fresh Views of Elliptical Galaxies, eds. A. Buzzoni, A. Renzini, & A. Serrano, 225
- Greggio, L., & Renzini, A. 1983, *A&A*, 118, 217
- Holweger, H. 2001, in *Solar and Galactic Composition*, ed. R.F. Wimmer-Schweingruber
- Idiart, T.P., Thevenin, F., & de Freitas Pacheco, J.A. 1997, *AJ*, 113, 1066
- Iwamoto, K., Barchwitz, F., Nomoto, K., Kishimoto, N., Umeda, H., Hix, W.R., Thielemann, F.K. 1999, *ApJSS*, 125, 439
- Jaffe, W., 1983, *MNRAS*, 202, 995
- Jimenez, R., Padoan, P., Matteucci, F., Heavens, A.F., 1998, *MNRAS*, 299, 123
- J rgensen, I. 1999, *MNRAS*, 306, 607
- Kauffmann, G., & Charlot, S. 1998, *MNRAS*, 294, 705
- Kauffmann, G., & White, S.D.M. 1993, *MNRAS*, 261, 921
- Kawata, D. 2001, *ApJ*, 558, 598
- Kawata, D., & Gibson, B.K. 2003, *MNRAS*, 340, 908
- Kobayashi, C., & Arimoto, N. 1999, *ApJ*, 527, 573
- Kodama, T., & Arimoto, N. 1997, *A&A*, 320, 41
- Kormendy, J., & Djorgovski, S. 1989, *ARA&A*, 27, 235
- Kuntschner, H. 2000, *MNRAS*, 315, 184
- Kuntschner, H., Lucey, J.R., Smith, R.J., Hudson, M.J., Davies, R.L. 2001, *MNRAS*, 323, 615
- Larson, R.B., 1974, *MNRAS*, 166, 585
- Martinelli, A., Matteucci, F., Colafrancesco, S., 1998, *MNRAS*, 298, 42
- Matteucci, F., 1992, *ApJ*, 397, 32
- Matteucci, F. 1994, *A&A*, 288, 57
- Matteucci, F. 2001, *The chemical evolution of the Galaxy*, Kluwer Academic Publishers, Dordrecht
- Matteucci, F., & Fran ois, P. 1989, *MNRAS*, 239, 885
- Matteucci, F., & Gibson, B.K., 1995, *A&A*, 304, 11
- Matteucci, F., & Greggio, L., 1986, *A&A*, 154, 279
- Matteucci, F., & Pipino, A. 2002, *ApJ*, 596, 69
- Matteucci, F., Ponzzone, R., Gibson, B.K., 1998, *A&A*, 335, 855
- Matteucci, F., & Tornambe', A., 1987, *A&A*, 185, 51
- Mehlert, D., Saglia, R.P., Bender, R., & Wegner, G. 2000, *A&AS*, 141, 449
- Mehlert, D., Thomas, D., Saglia, R.P., Bender, R., & Wegner, G. 2003, *A&A*, 407, 423
- Menanteau, F., Abraham, R.G., & Ellis, R.S. 2001a, *MNRAS*, 322, 1
- Menanteau, F., Jimenez, R., Matteucci, F. 2001b, *ApJ*, 562, 23
- Meynet, G., Maeder, A. 2002, *A&A*, 381, 25
- Miyazaki, M., Kodama, T., Okamura, S., et al. 2002, submitted to *ApJ*, astro-ph/0210509
- Mobasher, B., Guzman, R., Aragon-Salamanca, A., Zepf, S., 1999, *MNRAS*, 304, 225
- Nipoti, C., Londrillo, P., Ciotti, L. 2002, *MNRAS*, 332, 901
- Nipoti, C., Londrillo, P., Ciotti, L. 2003, proceedings of 'The mass of galaxies at low and high redshift' ESO workshop
- Nomoto, K., Hashimoto, M., Tsujimoto, T., Thielemann, F.K., Kishimoto, N., Kubo, Y., Nakasato, N., 1997, *Nuclear Physics A*, A621, 467
- O'Connell, R.W. 1976, *ApJ*, 206, 370
- Pagel, B.E.J., & Patchett, B.E. 1975, *MNRAS*, 172, 13
- Peebles, P.J.E. 2002, in *A New Era in Cosmology*, ASP Conference Series, eds. N.Metcalf & T.Shanks, in press
- Peletier, R.F., Davies, R.L., Illingworth, G.D., Davis, L.E., Cawson, M. 1990, *AJ*, 100, 1091
- Pipino, A., Matteucci, F., Borgani, S., Biviano, A. 2002, *NewA*, 7, 227
- Recchi, S., Matteucci, F., D'Ercole, A., 2001, *MNRAS*, 322, 800
- Renzini, A., & Cimatti, A. 1999, in 'The Hy-Redshift Universe: Galaxy Formation and Evolution at High Redshift', ASP Conference Proceedings, Vol. 193, A.J. Bunker and W.J.M. van Breugel eds.
- Renzini, A., & Ciotti, L. 1983, *ApJL*, 416, 49

- Romano, D., Silva, L., Matteucci, F., Danese, L. 2002, MNRAS, 334, 444
- Rusin, D., Kochanek, C.S., Falco, E.E., Keeton, C.R., McLeod, B.A., Impey, C.D., Lehar, J., Munoz, J.A., Peng, C.Y., Rix, H.W. 2003, ApJ, 587, 143
- Saglia, R.P., Maraston, C., Greggio, L., Bender, R., & Ziegler, B. 2000, 360, 911
- Saglia, R.P., Maraston, C., Thomas, D., Bender, R., & Colless, M. 2002, ApJ, 579, 13
- Salpeter, E.E., 1955, ApJ, 121, 161
- Scodreggio, M., Gavazzi, G., Belsole, E., Pierini, D., & Boselli, A. 1998, MNRAS, 301, 1001
- Stanford, S.A., Eisenhardt, P.R., & Dickinson, M. 1998, ApJ, 492, 461
- Steidel, C.C., Giavalisco, M., Pettini, M., Dickinson, M., & Adelberger, K.L., 1996a, ApJ, 462, L17
- Steidel, C.C., Giavalisco, M., Dickinson, M., Adelberger, K.L., 1996b, AJ, 112, 352
- Tamura, N., Kobayashi, C., Arimoto, N., Kodama, T., Ohta, K. 2000, AJ, 119, 2134
- Tantalo, R., Bressan, A., Chiosi, C., 1998a, A&A, 333, 419
- Tantalo, R., Chiosi, C., Bressan, A., Fagotto, F. 1996, A&A, 311, 361
- Tantalo, R., Chiosi, C., Bressan, A., Marigo, P., Portinari, L. 1998b, A&A, 335, 823
- Thielemann, F.K., Nomoto, K., Hashimoto, M. 1996, ApJ, 460, 408 (TNH96)
- Thomas, D., Greggio, L., & Bender, R., 1999, MNRAS, 302, 537
- Thomas, D., & Kauffmann, G. 1999, in Spectroscopic dating of stars and galaxies, ASP Conference Series, 192, eds. I. Hubeny, S. Heap, R. Cornett, 261
- Thomas, D., Maraston, C., & Bender, R., 2002, Ap&SS, 281, 371
- Thomas, D., Maraston, C., & Bender, R., 2003, MNRAS, 339, 897
- Tinsley, B.M., 1980, ApJ, 241, 41
- Trager, S.C., Faber, S.M., Worthey, G., Gonzalez, J.J., 2000a, AJ, 119, 1654
- Trager, S.C., Faber, S.M., Worthey, G., Gonzalez, J.J., 2000b, AJ, 120, 165
- Trager, S.C., Worthey, G., Faber, S.M., Burstein, D., Gonzalez, J.J., 1998 ApJS, 116, 1
- van de Ven, G., van Dokkum, P.G., Franx, M. 2003, MNRAS, 344, 924
- van den Hoek, L.B., Groenewegen, M.A.T. 1997, A&AS, 123, 305
- van Dokkum, P.G., & Franx, M. 1996, MNRAS, 281, 985
- van Dokkum, P.G., Franx, M., Kelson, D.D., Illingworth, G.D., Fisher, D., Fabricant, D. 1998, ApJ, 500, 714
- Weiss, A., Peletier, R.F., Matteucci, F. 1995, A&A, 296, 73
- Whelan, J., Iben, I. Jr. 1973, ApJ, 186, 1007
- White, S.D.M., & Rees, M.J., 1978, MNRAS, 183, 341
- Woosley, S.E., & Weaver, T.A., 1995, ApJS, 101, 181 (WW95)
- Worthey, G. 1994, ApJS, 95, 107
- Worthey, G. 1998, PASP, 110, 888
- Worthey, G., & Collobert, M. 2003, ApJ, 586, 17
- Worthey, G., Dorman, B., Jones, L.A. 1996, AJ, 112, 948
- Worthey, G., Faber, S.M., & Gonzalez, J.J. 1992, ApJ, 398, 69